Dynamics of a binary system around a supermassive black hole

Kei-ichi Maeda,[1,2] Priti Gupta,[3] and Hirotada Okawa[4]

[1]*Department of Physics, Waseda University, Shinjuku, Tokyo 169-8555, Japan*
[2]*Center for Gravitational Physics and Quantum Information, Yukawa Institute for Theoretical Physics, Kyoto University, 606-8502, Kyoto, Japan*
[3]*Department of Physics, Indian Institute of Science, Bangalore 560012, India*
[4]*Waseda Institute for Advanced Study (WIAS), 1-21-1 Nishi Waseda, Shinjuku-ku, Tokyo 169-0051, Japan*

(Received 4 April 2023; accepted 12 May 2023; published 16 June 2023)

We discuss the motion of a binary system around a supermassive black hole. Using Fermi-Walker transport, we construct a local inertial reference frame and set up a Newtonian binary system. Assuming a circular geodesic observer around a Schwarzschild black hole, we write down the equations of motion of a binary. Introducing a small acceleration of the observer, we remove the interaction terms between the center of mass (CM) of a binary and its relative coordinates. The CM follows the observer's orbit, but its motion deviates from an exact circular geodesic. We first solve the relative motion of a binary system, and then find the motion of the CM by the perturbation equations with the small acceleration. We show that von Zeipel-Lidov-Kozai (vZLK) oscillations appear when a binary is compact and the initial inclination is larger than a critical angle. In a hard binary system, vZLK oscillations are regular, whereas in a soft binary system, oscillations are irregular both in period and in amplitude, although stable. We find an orbital flip when the initial inclination is large. As for the motion of the CM, the radial deviations from a circular orbit become stable oscillations with very small amplitude.

DOI: 10.1103/PhysRevD.107.124039

I. INTRODUCTION

After the remarkable success of the LIGO-Virgo-KAGRA Collaboration [1,2], the study of gravitational wave (GW) emission has received a significant boost. The analysis of data (obtained through the first three observational runs) produced over a hundred confident detections [3,4] from binary black holes (BH), a binary neutron star (NS), and BH-NS systems, with more to follow in the next decade. The scientific insights emerging from the detections have significantly revolutionized our understanding of the sources. For instance, some notable events revealed heavier stellar-mass BHs [5], and their origin is still under discussion. Using the electromagnetic counterpart, we found that the speed of GWs is very close to the speed of light as predicted by the general theory of relativity [6]. With the increase in detections, we can probe more fundamental questions like testing theories of gravity in strong field regimes, finding the redshift distribution of BHs and their environment, and so on [7–11].

Unlocking the scientific potential of GWs depends on our theoretical knowledge. In order to filter the GW signal from the detector noise, it is necessary to model the predicted waveform accurately. Current observations are from isolated binary systems. It is possible, however, that nature will provide us with more exotic sources. This paper will examine a three-body system as one of the likely sources. The environment near supermassive black holes (SMBHs) in galactic nuclei comprises many stars and compact objects. A binary system could emerge in these surroundings, which composes a natural hierarchical triple system [12–17]. Recent LIGO events suggest the hierarchical systems as a possible dynamical formation channel of the heavy merging binary BHs [18–20].

In a hierarchical triple, the distance between two bodies (forming an "inner" binary) is much less than the distance to the third body. In 1910, von Zeipel explored the dynamics of restricted hierarchical triples, revealing a remarkable phenomenon [21], and in 1962, Kozai and Lidov independently rediscovered the same one [22,23] (known as von Zeipel-Lidov-Kozai [vZLK] resonance)—when the two orbits are inclined relative to each other, there is a periodic exchange between orbital eccentricity and relative inclination in secular timescale [24]. The orbital eccentricity can reach extreme values leading to large emissions of GWs [25–27].

There has been extensive work on dynamics of such systems based on Newtonian or post-Newtonian approximation [28–35]. Recently we also find many works focusing on gravitational waves from such systems [25–27,36–44]. It has been shown that vZLK resonance leaves an imprint on the waveform and lies in the detectable range of future space-based detectors like LISA and DECIGO. Indirect observation of GW from a triple system is also studied by analyzing the cumulative

shift of periastron time of a binary pulsar undergoing vZLK oscillations [45,46]. The presence of a heavier tertiary has been considered in previous studies [47,48] using double-averaged equations of motion to investigate relativistic effects such as de-Sitter and Lens-Thirring precessions. In particular, de Sitter precession of the inner orbital plane was modeled via analogy with spin effects. However, such a term occurs naturally in the derivation of our approach. An additional study also investigated 3-body PN (3BpN) secular effects in a hierarachical system with heavy third body using a multiple scale method [49]. Also, they pointed out that 3BpN effects affected the evolution of these triples, resulting in a wider range of eccentricity and inclination.

In this paper, when we discuss on a binary system near SMBH, we follow another approach, i.e., a binary system is treated as perturbations of SMBH spacetime. In the case of a single object in SMBH spacetime, it can be treated as a test particle. But in the case of a binary system, this is not the case because the self-gravitational mutual interaction is much stronger than the gravitational tidal force by SMBH. In order to analyze such a hierarchical system, we first prepare a local inertial frame and set up a binary in this frame. When a binary is tightly bounded but the mutual gravitational interaction is not so strong, the binary motion in this frame can be discussed using Newtonian gravitational dynamics.

Using the Fermi normal coordinate system or Fermi-Walker transport, we can construct a local inertial frame [50–52]. Using such a technique, there are several discussions on a tidal force acting on stars near SMBH [53–56], but only a few works on a binary system have been discussed [57–59]. In this paper, we analyze such a system in detail. Assuming an observer is moving along a circular geodesic around a Schwarzschild SMBH, we construct a local inertial frame, and set up a binary system. We then discuss the motion of a binary, showing the existence of the vZLK oscillations when a binary is compact and the initial inclination angle is larger than a critical value.

The paper is organized as follows: We review how to construct a local inertial proper reference frame by use of Fermi-Walker transport in Sec. II A. In Sec. II B, we perform post-Newtonian expansion for a test particle motion in this frame. In Sec. III, we set up a self-gravitating system in the proper reference frame and derive the Lagrangian in the Newtonian limit. In Sec. IV, assuming an observer moving along a circular geodesic in Schwarzschild black hole, we derive the equations of motion for a binary system. We also discuss the interaction terms between the center of mass (CM) of a binary and its relative coordinates. Introducing small acceleration of an observer, we remove the interaction terms, finding the equations of motion for the CM, which gives small deviations from a circular geodesic. We then analyze twelve models numerically and show the properties of binary motions such as the vZLK oscillations, chaotic features, and orbital flips in Sec. V. We also discuss motions of the CM of a binary. Concluding remarks follow in Sec. VI. In the Appendix A, we provide some numerical and analytic solutions in the coplanar case. We also present the Lagrange planetary equations of the model and write down the equations for the orbital parameters of a binary taking averages over inner and outer binary cycles in Appendix B. We show that this simplified method recovers numerical results obtained by direct integration of the equations of motion in the case of a hard binary. It also provides the vZLK oscillation timescale and the maximum and minimum values of eccentricity.

Notation used: Greek letters range from 0 to 3, while Roman letters run from 1 to 3; hatted indices denote tetrad components in a proper reference frame rotating along an observer; bars over symbols correspond to quantities in a static tetrad frame.

II. PROPER REFERENCE FRAME

A. Proper reference frame of an arbitrary observer in a curved spacetime

We first discuss how to set up a local inertial frame in a curved spacetime [50,57,60]. The spacetime metric is given by

$$d\bar{s}^2 = \bar{g}_{\mu\nu} dx^\mu dx^\nu. \tag{2.1}$$

We then consider an observer, whose orbit is given by a world line γ described by

$$x^\mu = z^\mu(\tau),$$

where τ is a proper time of the observer. The 4-velocity is given by

$$u^\mu(\tau) \equiv \frac{dz^\mu}{d\tau}.$$

We now set up an orthonormal tetrad system $\{e^\mu_{\hat{\alpha}}\}$ along the observer's world line γ, which is defined by the conditions such that

$$e_{\hat{\alpha}}{}^\mu e_{\hat{\beta}\mu} = \eta_{\hat{\alpha}\hat{\beta}}, \qquad e_{\hat{0}}{}^\mu = u^\mu,$$

where $\eta_{\hat{\alpha}\hat{\beta}}$ is a Minkowski spacetime metric.

For a given 4-velocity u^μ, this tetrad system is determined up to three-dimensional rotations. The tetrad $e^\mu_{\hat{\alpha}}$ is transported along the observer's world line γ as

$$\frac{De^\mu_{\hat{i}}}{d\tau} = -\Omega^{\mu\nu} e_{\hat{i}\nu},$$

where

$$\Omega^{\mu\nu} \equiv a^\mu u^\nu - u^\mu a^\nu + u_\alpha \omega_\beta \epsilon^{\alpha\beta\mu\nu}.$$

Here,

$$a^\mu \equiv \frac{Du^\mu}{d\tau},$$

and

$$\omega_\mu \equiv \frac{1}{2} u^\alpha \epsilon_{\alpha\mu\rho\sigma}\Omega^{\rho\sigma} = \frac{1}{2} \overset{(3)}{\epsilon}_{\mu\rho\sigma}\Omega^{\rho\sigma},$$

are the acceleration of the observer and the angular velocity of a rotating spatial basis vector $e^\mu_{(a)}$, respectively. A nonrotating tetrad frame for which $\omega^\mu = 0$ is called the Fermi-Walker transport. If the orbit is a geodesic ($a^\mu = 0$ and $\omega^{\hat{k}} = 0$), we find $\frac{De^\mu_{\hat{a}}}{d\tau} = 0$, which is just a parallel transport.

Next, we construct a local coordinate system (the observer's proper reference system) near the world line γ, which is described as

$$(x^{\hat{\mu}}) = (c\tau, x^{\hat{a}}),$$

where the spatial component $x^{\hat{a}}$ is measured from the point at τ on the world line γ along the spatial hypersurface $\Sigma(\tau)$ perpendicular to γ.

We find that the metric form of this proper reference frame up to the second order of $x^{\hat{a}}$ is given by

$$g_{\hat{\mu}\hat{\nu}} = \eta_{\hat{\mu}\hat{\nu}} + \varepsilon_{\hat{\mu}\hat{\nu}} + O(|x^{\hat{k}}|^3), \tag{2.2}$$

where

$$\varepsilon_{\hat{0}\hat{0}} = -\frac{1}{c^2}\left[2a_{\hat{k}}x^{\hat{k}} + (c^2\bar{\mathcal{R}}_{\hat{0}\hat{k}\hat{0}\hat{\ell}} - \omega_{\hat{j}\hat{k}}\omega^{\hat{j}}{}_{\hat{\ell}})x^{\hat{k}}x^{\hat{\ell}} + \frac{(a_{\hat{k}}x^{\hat{k}})^2}{c^2}\right], \tag{2.3}$$

$$\varepsilon_{\hat{0}\hat{j}} = -\frac{1}{c^2}\left[c\omega_{\hat{j}\hat{k}}x^{\hat{k}} + \frac{2}{3}c^2\bar{\mathcal{R}}_{\hat{0}\hat{k}\hat{j}\hat{\ell}}x^{\hat{k}}x^{\hat{\ell}}\right], \tag{2.4}$$

$$\varepsilon_{\hat{i}\hat{j}} = -\frac{1}{c^2}\left[\frac{1}{3}c^2\bar{\mathcal{R}}_{\hat{i}\hat{k}\hat{j}\hat{\ell}}x^{\hat{k}}x^{\hat{\ell}}\right]. \tag{2.5}$$

$\bar{\mathcal{R}}_{\hat{\mu}\hat{\nu}\hat{\rho}\hat{\sigma}}$ is the tetrad component of the Riemann curvature of a background spacetime and $\omega_{\hat{j}\hat{k}} \equiv \epsilon_{\hat{j}\hat{k}\hat{\ell}}\omega^{\hat{\ell}}$ [50,57,60].

The acceleration and angular frequency in the proper reference frame are defined by

$$a^{\hat{j}} \equiv e^{\hat{j}}{}_\mu \frac{Du^\mu}{d\tau},$$
$$\omega^{\hat{j}} \equiv \frac{1}{2}\overset{(3)}{\epsilon}{}^{\hat{j}\hat{k}\hat{\ell}} e_{\hat{\ell}\mu}\frac{De^\mu_{\hat{k}}}{d\tau}.$$

For the Fermi-Walker transport, $\omega^{\hat{k}} = 0$. If it is the geodesic ($a^{\hat{j}} = 0$ and $\omega^{\hat{k}} = 0$), we recover the Fermi normal coordinates. The tetrad is parallelly transformed along the world line.

B. Test particle motion in a proper reference frame

First, we consider the motion of a test particle in the above proper reference frame. The action for a test particle with mass m in a given spacetime is given by

$$S = -mc\int\sqrt{-ds^2}.$$

For a test particle in the proper reference frame, since the world interval ds^2 is given by the metric $g_{\hat{\mu}\hat{\nu}}$, we find the action for a test particle to be

$$S = \int d\tau\mathcal{L},$$

where

$$\mathcal{L} \equiv -mc\sqrt{-(\eta_{\hat{\mu}\hat{\nu}} + \varepsilon_{\hat{\mu}\hat{\nu}})\frac{dx^{\hat{\mu}}}{d\tau}\frac{dx^{\hat{\nu}}}{d\tau}},$$

is Lagrangian of the test particle and $\varepsilon_{\hat{\mu}\hat{\nu}}$ is a small deviation from the Minkowski spacetime since $|\varepsilon_{\hat{\mu}\hat{\nu}}| \ll 1$.

Assuming that the test particle moves slowly in the proper reference frame, we perform the post-Newtonian expansion in terms of $v^{\hat{j}}/c$ as follows: First, we expand the square root term in the Lagrangian as

$$\begin{aligned}\mathcal{L} &= -mc^2\sqrt{1 - \frac{\boldsymbol{v}^2}{c^2} - \varepsilon_{\hat{0}\hat{0}} - 2\varepsilon_{\hat{0}\hat{j}}\frac{v^{\hat{j}}}{c} - \varepsilon_{\hat{i}\hat{j}}\frac{v^{\hat{i}}v^{\hat{j}}}{c^2}} \\ &= -mc^2\left\{1 - \frac{\boldsymbol{v}^2}{2c^2} - \frac{\varepsilon_{\hat{0}\hat{0}}}{2} - \varepsilon_{\hat{0}\hat{j}}\frac{v^{\hat{j}}}{c} - \frac{1}{2}\varepsilon_{\hat{i}\hat{j}}\frac{v^{\hat{i}}v^{\hat{j}}}{c^2}\right. \\ &\quad \left. - \frac{1}{8}\left[\frac{\boldsymbol{v}^2}{c^2} + \varepsilon_{\hat{0}\hat{0}} + 2\varepsilon_{\hat{0}\hat{j}}\frac{v^{\hat{j}}}{c} + \varepsilon_{\hat{i}\hat{j}}\frac{v^{\hat{i}}v^{\hat{j}}}{c^2}\right]^2 + \cdots\right\}.\end{aligned}$$

Note that $x^{\hat{0}} = c\tau$. Inserting Eqs. (2.3), (2.4), and (2.5), and expanding the above Lagrangian in terms of $v^{\hat{j}}/c$, we obtain

$$\mathcal{L} = \mathcal{L}_0 + \mathcal{L}_{1/2} + \mathcal{L}_1,$$

where

$$\mathcal{L}_0 = \frac{1}{2}m\boldsymbol{v}^2 - ma_{\hat{k}}x^{\hat{k}} - \frac{1}{2}m\omega_{\hat{j}\hat{k}}\omega^{\hat{j}}{}_{\hat{\ell}}x^{\hat{k}}x^{\hat{\ell}} - m\omega_{\hat{j}\hat{k}}v^{\hat{j}}x^{\hat{k}} - \frac{1}{2}mc^2\bar{\mathcal{R}}_{\hat{0}\hat{k}\hat{0}\hat{\ell}}x^{\hat{k}}x^{\hat{\ell}},$$

$$\mathcal{L}_{1/2} = -\frac{2}{3}mc^2\bar{\mathcal{R}}_{\hat{0}\hat{k}\hat{j}\hat{\ell}}x^{\hat{k}}x^{\hat{\ell}}\frac{v^{\hat{j}}}{c},$$

$$\mathcal{L}_1 = -\frac{m}{2}\frac{(a_{\hat{k}}x^{\hat{k}})^2}{c^2} - \frac{1}{6}mc^2\bar{\mathcal{R}}_{\hat{i}\hat{k}\hat{j}\hat{\ell}}x^{\hat{k}}x^{\hat{\ell}}\frac{v^{\hat{i}}v^{\hat{j}}}{c^2} + \frac{m}{8c^2}\left[\boldsymbol{v}^2 - 2a_{\hat{k}}x^{\hat{k}} - \omega_{\hat{j}\hat{k}}\omega^{\hat{j}}_{\hat{l}}x^{\hat{k}}x^{\hat{\ell}} - 2\omega_{\hat{j}\hat{k}}x^{\hat{k}}v^{\hat{j}} - c^2\bar{\mathcal{R}}_{\hat{0}\hat{k}\hat{0}\hat{\ell}}x^{\hat{k}}x^{\hat{\ell}}\right]^2,$$

are Newtonian, 0.5 PN and 1PN Lagrangian, respectively.

In this expansion, we find the 0.5 PN term formally, but it can be an apparent term which comes from a choice of an observer's coordinates. In fact, if we choose an appropriate observer's acceleration, which appears as a 0.5 PN term, we can remove the above $\mathcal{L}_{1/2}$. However, if we have a multiparticle system as we will discuss later, this adjustment can be used only for one particle or the center of mass of the system (See Sec. III). Hence, we keep the $\mathcal{L}_{1/2}$ term and discuss "Newtonian" dynamics including such a term.

III. SELF-GRAVITATING NEWTONIAN SYSTEM IN A CURVED SPACETIME

A. Self-gravitating N-body system

Now we discuss self-gravitating N-body system in a fixed curved background spacetime, which is given by the metric in Eq. (2.1) [57]. We are interested in the case where Newtonian dynamics is valid in the observer's proper reference frame. The necessary condition is that the typical scale $\ell_{N\text{-body}}$ of N-body system should satisfy

$$\ell_{N\text{-body}} \ll \min\left[\frac{1}{|a^{\hat{j}}|}, \frac{1}{|\omega^{\hat{j}}|}, \ell_{\bar{\mathcal{R}}}\right],$$

where $\ell_{\bar{\mathcal{R}}}$ is the minimum curvature radius defined by

$$\ell_{\bar{\mathcal{R}}} \equiv \min\left[|\bar{\mathcal{R}}_{\hat{\mu}\hat{\nu}\hat{\rho}\hat{\sigma}}|^{-\frac{1}{2}}, |\bar{\mathcal{R}}_{\hat{\mu}\hat{\nu}\hat{\rho}\hat{\sigma};\hat{\alpha}}|^{-\frac{1}{3}}, |\bar{\mathcal{R}}_{\hat{\mu}\hat{\nu}\hat{\rho}\hat{\sigma};\hat{\alpha}\hat{\beta}}|^{-\frac{1}{4}}\right].$$

In order to find the metric contributions from N-body system, we first focus on the motion of the Ith particle, which is gravitating with the other $(N-1)$ particles. The metric contribution from the those $(N-1)$ particles is given by

$$\varphi^I_{\hat{0}\hat{0}} = -\frac{2\Phi_I}{c^2},$$

where Φ_I is the Newtonian potential produced by the $(N-1)$ particles, which is given by

$$\Phi_I(x^{\hat{i}}) = -G\sum_{J\neq I}^{N}\frac{m_J}{|x^{\hat{i}} - x^{\hat{i}}{}_J|}.$$

We assume that the other components of $\varphi^I_{\hat{\mu}\hat{\nu}}$ vanish because we are interested in Newtonian dynamics in the proper reference frame.

We then obtain the metric of the observer's proper reference frame for the Ith particle as

$$g^I_{\hat{\mu}\hat{\nu}} = \eta_{\hat{\mu}\hat{\nu}} + h^I_{\hat{\mu}\hat{\nu}}, \tag{3.1}$$

where

$$h^I_{\hat{\mu}\hat{\nu}} = \varepsilon_{\hat{\mu}\hat{\nu}} + \varphi^I_{\hat{\mu}\hat{\nu}}. \tag{3.2}$$

The equation of motion for the Ith particle can be derived by the variation of the action

$$\mathcal{S}_I = \int d\tau\mathcal{L}_I,$$

where

$$\mathcal{L}_I \equiv -m_Ic\sqrt{-g^I_{\hat{\mu}\hat{\nu}}\frac{dx^{\hat{\mu}}_I}{d\tau}\frac{dx^{\hat{\nu}}_I}{d\tau}}.$$

By use of the metric form (3.1), we can expand the above Lagrangian up to 0.5 PN order as

$$\mathcal{L}_I = \frac{1}{2}m_I\left(\frac{d\boldsymbol{x}_I}{d\tau}\right)^2 - m_I\Phi(x_I) - m_Ia_{\hat{k}}x^{\hat{k}}_I - \frac{1}{2}m_I\omega_{\hat{j}\hat{k}}\omega^{\hat{j}}_{\hat{\ell}}x^{\hat{k}}_Ix^{\hat{\ell}}_I - m_I\omega_{\hat{j}\hat{k}}v^{\hat{j}}_Ix^{\hat{k}}_I - \frac{1}{2}m_Ic^2\bar{\mathcal{R}}_{\hat{0}\hat{k}\hat{0}\hat{\ell}}x^{\hat{k}}_Ix^{\hat{\ell}}_I - \frac{2}{3}m_Ic^2\bar{\mathcal{R}}_{\hat{0}\hat{k}\hat{j}\hat{\ell}}x^{\hat{k}}_Ix^{\hat{\ell}}_I\frac{v^{\hat{j}}_I}{c}.$$

The total action of N-body system and its Lagrangian are given by summing up each Lagrangian $\mathcal{L}_I$. We finally obtain

$$\mathcal{S}_{N\text{-body}} = \int d\tau\mathcal{L}_{N\text{-body}},$$

where

$$\mathcal{L}_{N\text{-body}} = \frac{1}{2}\sum_I m_I\left(\frac{d\boldsymbol{x}_I}{d\tau}\right)^2 + \sum_I^N\sum_{J\neq I}^N \frac{Gm_Im_J}{2|x^{\hat{i}}_I - x^{\hat{i}}{}_J|} + \mathcal{L}_a + \mathcal{L}_\omega + \mathcal{L}_{\bar{\mathcal{R}}},$$

with

$$\mathcal{L}_a = -\sum_I^N m_I a_{\hat{k}} x^{\hat{k}}_I,$$

$$\mathcal{L}_\omega = -\frac{1}{2}\sum_I^N m_I\left[\omega_{\hat{j}\hat{k}}\omega^{\hat{j}}{}_{\hat{\ell}} x^{\hat{k}}_I x^{\hat{\ell}}_I + 2\omega_{\hat{j}\hat{k}} v^{\hat{j}}_I x^{\hat{k}}_I\right],$$

$$\mathcal{L}_{\bar{\mathcal{R}}} = -\frac{1}{2}\sum_I^N m_I c^2 \bar{\mathcal{R}}_{\hat{0}\hat{k}\hat{0}\hat{\ell}} x^{\hat{k}}_I x^{\hat{\ell}}_I - \frac{2}{3}\sum_I m_I c^2 \bar{\mathcal{R}}_{\hat{0}\hat{k}\hat{j}\hat{\ell}} x^{\hat{k}}_I x^{\hat{\ell}}_I \frac{v^{\hat{j}}_I}{c}.$$

Note that $\mathcal{L}_a$ comes from the inertial force of the accelerated observer, and $\mathcal{L}_\omega$ originates in the rotation of the observer (the centrifugal force and the Coriolis force). $\mathcal{L}_{\bar{\mathcal{R}}}$ describes the curvature effect of the third body (the tidal force).

B. Binary system in a curved spacetime

Next, we discuss a binary system in a fixed curved background. A binary consists of two point particles with the masses m_1 and m_2. The Lagrangian up to 0.5 PN order is given by

$$\mathcal{L}_{\text{binary}} = \mathcal{L}_{\text{N}} + \mathcal{L}_{1/2}, \tag{3.3}$$

where

$$\mathcal{L}_{\text{N}} \equiv \frac{1}{2}\left[m_1\left(\frac{d\boldsymbol{x}_1}{d\tau}\right)^2 + m_2\left(\frac{d\boldsymbol{x}_2}{d\tau}\right)^2\right] + \frac{Gm_1m_2}{|\boldsymbol{x}_1 - \boldsymbol{x}_2|} + \mathcal{L}_a + \mathcal{L}_\omega + \mathcal{L}_{\bar{\mathcal{R}}}, \tag{3.4}$$

with

$$\mathcal{L}_a = -\sum_{I=1}^2 m_I a_{\hat{k}} x^{\hat{k}}_I,$$

$$\mathcal{L}_\omega = -\sum_{I=1}^2 m_I\left[\epsilon_{\hat{j}\hat{k}\hat{\ell}}\omega^{\hat{\ell}} x^{\hat{k}}_I \frac{dx^{\hat{j}}_I}{d\tau} - \frac{1}{2}(\boldsymbol{\omega}^2\boldsymbol{x}_I^2 - (\boldsymbol{\omega}\cdot\boldsymbol{x}_I)^2)\right],$$

$$\mathcal{L}_{\bar{\mathcal{R}}} = -\frac{1}{2}\sum_{I=1}^2 m_I \bar{\mathcal{R}}_{\hat{0}\hat{k}\hat{0}\hat{\ell}} x^{\hat{k}}_I x^{\hat{\ell}}_I,$$

and

$$\mathcal{L}_{1/2} \equiv -\frac{2}{3}\sum_{I=1}^2 m_I c^2 \bar{\mathcal{R}}_{\hat{0}\hat{k}\hat{j}\hat{\ell}} x^{\hat{k}}_I x^{\hat{\ell}}_I \frac{v^{\hat{j}}_I}{c}. \tag{3.5}$$

Introducing the center of mass coordinates and the relative coordinates by

$$\boldsymbol{R} = \frac{m_1\boldsymbol{x}_1 + m_2\boldsymbol{x}_2}{m_1 + m_2},$$
$$\boldsymbol{r} = \boldsymbol{x}_2 - \boldsymbol{x}_1,$$

we find the Newtonian Lagrangian [Eq. (3.4)] in terms of $\boldsymbol{R}$ and $\boldsymbol{r}$ as

$$\mathcal{L}_{\text{N}} = \mathcal{L}_{\text{CM}}(\boldsymbol{R},\dot{\boldsymbol{R}}) + \mathcal{L}_{\text{rel}}(\boldsymbol{r},\dot{\boldsymbol{r}}), \tag{3.6}$$

where

$$\mathcal{L}_{\text{CM}}(\boldsymbol{R},\dot{\boldsymbol{R}}) = \frac{1}{2}(m_1 + m_2)\dot{\boldsymbol{R}}^2 + \mathcal{L}_{\text{CM-}a}(\boldsymbol{R},\dot{\boldsymbol{R}}) + \mathcal{L}_{\text{CM-}\omega}(\boldsymbol{R},\dot{\boldsymbol{R}}) + \mathcal{L}_{\text{CM-}\bar{\mathcal{R}}}(\boldsymbol{R},\dot{\boldsymbol{R}}),$$

with

$$\mathcal{L}_{\text{CM-}a} = -(m_1 + m_2)a_{\hat{k}} x^{\hat{k}}_I,$$

$$\mathcal{L}_{\text{CM-}\omega} = -(m_1 + m_2)\left[\epsilon_{\hat{j}\hat{k}\hat{\ell}}\omega^{\hat{\ell}} R^{\hat{k}}\dot{R}^{\hat{j}} - \frac{1}{2}(\boldsymbol{\omega}^2\boldsymbol{R}^2 - (\boldsymbol{\omega}\cdot\boldsymbol{R})^2)\right],$$

$$\mathcal{L}_{\text{CM-}\bar{\mathcal{R}}} = -\frac{1}{2}(m_1 + m_2)\bar{\mathcal{R}}_{\hat{0}\hat{k}\hat{0}\hat{\ell}} R^{\hat{k}} R^{\hat{\ell}},$$

and

$$\mathcal{L}_{\text{rel}}(\boldsymbol{r},\dot{\boldsymbol{r}}) = \frac{1}{2}\mu\dot{\boldsymbol{r}}^2 + \frac{Gm_1m_2}{r} + \mathcal{L}_{\text{rel-}\omega}(\boldsymbol{r},\dot{\boldsymbol{r}}) + \mathcal{L}_{\text{rel-}\bar{\mathcal{R}}}(\boldsymbol{r},\dot{\boldsymbol{r}}),$$

with

$$\mathcal{L}_{\text{rel-}\omega} = -\mu\left[\epsilon_{\hat{j}\hat{k}\hat{\ell}}\omega^{\hat{\ell}} r^{\hat{k}}\dot{r}^{\hat{j}} - \frac{1}{2}(\boldsymbol{\omega}^2\boldsymbol{r}^2 - (\boldsymbol{\omega}\cdot\boldsymbol{r})^2)\right],$$

$$\mathcal{L}_{\text{rel-}\bar{\mathcal{R}}} = -\frac{1}{2}\mu\bar{\mathcal{R}}_{\hat{0}\hat{k}\hat{0}\hat{\ell}} r^{\hat{k}} r^{\hat{\ell}}.$$

Here, $\mu = m_1m_2/(m_1 + m_2)$ is the reduced mass. When we consider only $\mathcal{L}_{\text{N}}$, we can separate the variables $\boldsymbol{R}$ and $\boldsymbol{r}$. In particular, when the observer follows the geodesic ($\boldsymbol{a} = 0$ and $\boldsymbol{\omega} = 0$), the orbit of $\boldsymbol{R} = 0$ is a solution of the equation for $\boldsymbol{R}$. It means that the center of mass (CM) follows the observer's geodesic. We have only the equation for the relative coordinate $\boldsymbol{r}$. However, when we include the 0.5 PN term, it is not the case. The 0.5 PN Lagrangian $\mathcal{L}_{1/2}$ is rewritten by use of $\boldsymbol{R}$ and $\boldsymbol{r}$ as

$$\mathcal{L}_{1/2} = \mathcal{L}_{1/2\text{-CM}}(\boldsymbol{R},\dot{\boldsymbol{R}}) + \mathcal{L}_{1/2\text{-rel}}(\boldsymbol{r},\dot{\boldsymbol{r}}) + \mathcal{L}_{1/2\text{-int}}(\boldsymbol{R},\dot{\boldsymbol{R}},\boldsymbol{r},\dot{\boldsymbol{r}}), \tag{3.7}$$

where

$$\mathcal{L}_{1/2\text{-CM}}(\boldsymbol{R},\dot{\boldsymbol{R}}) = -\frac{2}{3}(m_1+m_2)R_{\hat{0}\hat{k}\hat{j}\hat{\ell}}R^{\hat{k}}R^{\hat{\ell}}\dot{R}^{\hat{j}},$$

$$\mathcal{L}_{1/2\text{-rel}}(\boldsymbol{r},\dot{\boldsymbol{r}}) = -\frac{2}{3}\mu\frac{(m_1-m_2)}{(m_1+m_2)}R_{\hat{0}\hat{k}\hat{j}\hat{\ell}}r^{\hat{k}}r^{\hat{\ell}}\dot{r}^{\hat{j}},$$

$$\mathcal{L}_{1/2\text{-int}}(\boldsymbol{R},\dot{\boldsymbol{R}},\boldsymbol{r},\dot{\boldsymbol{r}}) = -\frac{2}{3}\mu R_{\hat{0}\hat{k}\hat{j}\hat{\ell}} \times\left[r^{\hat{k}}r^{\hat{\ell}}\dot{R}^{\hat{j}} + (R^{\hat{k}}r^{\hat{\ell}\hat{j}} + r^{\hat{k}}R^{\hat{\ell}})\dot{r}^{\hat{j}}\right]. \quad (3.8)$$

Due to the interaction term $\mathcal{L}_{1/2\text{-int}}$, the orbit of $\boldsymbol{R}=0$ is no longer a solution even if the acceleration vanishes. The motion of the CM $[\boldsymbol{R}(\tau)]$ couples with the relative motion $(\boldsymbol{r}(\tau))$. As a result, not only the orbit of a binary but also the motion of the CM will become complicated even if the observer's orbit is a geodesic.

However, if we introduce an appropriate acceleration $\boldsymbol{a}$ in 0.5 PN order to cancel the interaction terms, $\boldsymbol{R}=0$ will become a solution, i.e., the CM can follow the observer's motion as follows: Integrating by parts the interaction term, we find

$$\mathcal{L}_{1/2\text{-int}}(\boldsymbol{R},\dot{\boldsymbol{R}},\boldsymbol{r},\dot{\boldsymbol{r}}) = -\frac{2}{3}\mu\bar{\mathcal{R}}_{\hat{0}\hat{k}\hat{j}\hat{\ell}}\left[\dot{R}^{\hat{j}}r^{\hat{k}}r^{\hat{\ell}} + \dot{r}^{\hat{j}}(R^{\hat{k}}r^{\hat{\ell}} + r^{\hat{k}}R^{\hat{\ell}})\right] \approx 2\mu\left[\frac{1}{3}\frac{d\bar{\mathcal{R}}_{\hat{0}\hat{k}\hat{j}\hat{\ell}}}{d\tau}r^{\hat{k}}r^{\hat{\ell}} + \bar{\mathcal{R}}_{\hat{0}\hat{k}\hat{j}\hat{\ell}}r^{\hat{k}}\dot{r}^{\hat{\ell}}\right]R^{\hat{j}}$$

(integration by part),

where the time derivative of the curvature is evaluated along the observer's orbit.

If we define the acceleration by

$$a_{\hat{j}} = \frac{2\mu}{m_1+m_2}\left[\frac{1}{3}\frac{d\bar{\mathcal{R}}_{\hat{0}\hat{k}\hat{j}\hat{\ell}}}{d\tau}r^{\hat{k}}r^{\hat{\ell}} + \bar{\mathcal{R}}_{\hat{0}\hat{k}\hat{j}\hat{\ell}}r^{\hat{k}}\dot{r}^{\hat{\ell}}\right],$$

two terms $\mathcal{L}_{1/2\text{-int}}$ and $\mathcal{L}_{\text{CM-}a}$ cancel each other. As a result, the Lagrangians for $\boldsymbol{R}$ and $\boldsymbol{r}$ are decoupled, and $\boldsymbol{R}=0$ becomes an exact solution of the equation for $\boldsymbol{R}$, which is derived from the Lagrangian $(\mathcal{L}_{\text{CM}}+\mathcal{L}_{1/2\text{-CM}})$. The CM follows the observer's orbit and therefore, we obtain the decoupled equation for the relative coordinate $\boldsymbol{r}$.

In order to obtain the proper observer's orbit, which is not a geodesic but close to the geodesic[1], we have to solve the equation of motion including small acceleration such that

$$\frac{Du^{\mu}_{\text{CM}}}{d\tau} = a^{\mu} = e^{\mu\hat{j}}a_{\hat{j}} = \frac{2\mu}{m_1+m_2}e^{\mu\hat{j}}\left[\frac{1}{3}\frac{d\bar{\mathcal{R}}_{\hat{0}\hat{k}\hat{j}\hat{\ell}}}{d\tau}r^{\hat{k}}r^{\hat{\ell}} + \bar{\mathcal{R}}_{\hat{0}\hat{k}\hat{j}\hat{\ell}}r^{\hat{k}}\dot{r}^{\hat{\ell}}\right]. \quad (3.9)$$

Note that the second term in the acceleration corresponds to the gravitomagnetic force given in [58].

[1]When initial deviation is small, this is confirmed by perturbation analysis as shown later.

As a result, we first solve the equation for the relative coordinate $\boldsymbol{r}$, which is obtained only by the Lagrangian $\mathcal{L}_{\text{rel}}(\boldsymbol{r})+\mathcal{L}_{1/2\text{-rel}}(\boldsymbol{r})$. Note that when $m_1=m_2$, we have only Newtonian Lagrangian $\mathcal{L}_{\text{rel}}$ because $\mathcal{L}_{1/2\text{-rel}}=0$ vanishes. After obtaining the solution of $\boldsymbol{r}(\tau)$, we find the motion for the CM (or the observer) in the background spacetime by solving Eq. (3.9). Using the relative motion $\boldsymbol{r}(\tau)$ with the solution of the CM motion $[x^{\mu}_{\text{CM}}(\tau)]$, we will obtain a binary motion in a given curved background spacetime $[x^{\mu}_1(\tau), x^{\mu}_2(\tau)]$.

IV. A BINARY SYSTEM IN A SCHWARZSCHILD SPACETIME

We consider a spherically symmetric supermassive black hole. The background spacetime is given by the Schwarzschild solution as

$$d\bar{s}^2 = -f d\mathfrak{t}^2 + \frac{1}{f}d\mathfrak{r}^2 + \mathfrak{r}^2 d\Omega^2, \quad (4.1)$$

where

$$f = 1 - \frac{\mathfrak{r}_g}{\mathfrak{r}}. \quad (4.2)$$

The gravitational radius $\mathfrak{r}_g$ is given by

$$\mathfrak{r}_g \equiv \frac{2GM}{c^2},$$

where M is a gravitational mass of the supermassive black hole. In what follows, we set $G=1$ and $c=1$ for brevity unless specified otherwise.

A. Proper reference frame

We first discuss Newtonian dynamics for which Lagrangian $\mathcal{L}_{\text{N}}$ is given by Eq. (3.4). In this case, the CM of a binary system follows a geodesic observer. We consider an observer, which moves along a circular geodesic with the radius $\mathfrak{r}=\mathfrak{r}_0$. The orbit is assumed to be on the equatorial plane without loss of generality. We introduce a rotating tetrad system along this geodesic such that

$$e_{\hat{0}}{}^{\mu} \equiv u^{\mu} = \left(\frac{\sqrt{1+\mathfrak{r}_0^2\mathfrak{w}_0^2}}{\sqrt{f(\mathfrak{r}_0)}}, 0, 0, \mathfrak{w}_0\right),$$

$$e_{\hat{1}}{}^{\mu} = (0, \sqrt{f(\mathfrak{r}_0)}, 0, 0),$$

$$e_{\hat{2}}{}^{\mu} = \left(\frac{\mathfrak{r}_0\mathfrak{w}_0}{\sqrt{f(\mathfrak{r}_0)}}, 0, 0, \frac{\sqrt{1+\mathfrak{r}_0^2\mathfrak{w}_0^2}}{\mathfrak{r}_0}\right),$$

$$e_{\hat{3}}{}^{\mu} = \left(0, 0, -\frac{1}{\mathfrak{r}_0}, 0\right),$$

where the angular frequency $\mathfrak{w}_0$ is defined by

$$\mathfrak{w}_0 = u^3 = \frac{d\varphi}{d\tau} = \frac{1}{\mathfrak{r}_0(\mathfrak{r}_0/M-3)^{1/2}}. \tag{4.3}$$

We then calculate the angular velocity $\omega^{\hat{j}}$ of this rotating tetrad system as

$$\omega^{\hat{j}} = \frac{1}{2}\,{}^{(3)}\epsilon^{\hat{j}\hat{k}\hat{\ell}}\, e_{\hat{\ell}\mu}\frac{De_{\hat{k}}{}^{\mu}}{d\tau} = \mathfrak{w}_{\mathrm{R}}\delta^{\hat{j}}{}_{\hat{3}},$$

where

$$\mathfrak{w}_{\mathrm{R}} = \frac{1}{\mathfrak{r}_0(\mathfrak{r}_0/M)^{1/2}}, \tag{4.4}$$

is the angular frequency of the rotating tetrad frame (See Fig. 1). Note that this angular frequency is different from the observer's angular frequency $\mathfrak{w}_0$. The difference between two angular frequencies $\mathfrak{w}_0$ and $\mathfrak{w}_R$, i.e.,

$$\mathfrak{w}_{\mathrm{dS}} \equiv \mathfrak{w}_0 - \mathfrak{w}_{\mathrm{R}} \tag{4.5}$$

describes the rotation of a nonrotating inertial frame moving along a circular orbit, which may cause de Sitter precession [61]. In fact, when $\mathfrak{r}_0 \gg \mathfrak{r}_g$, we find

$$\mathfrak{w}_{\mathrm{dS}} \approx \frac{3M^{3/2}}{2\mathfrak{r}_0^{5/2}},$$

which is the same as de Sitter frequency $\Omega^{(GR)}_{L_{\mathrm{in}}L_{\mathrm{out}}}$ given in [48] in the limit of $M \gg m_1, m_2$.

Next, we calculate the Riemann curvature in the above tetrad system. In the static tetrad system $\{e^{\bar{\alpha}}{}_{\mu}\}$ with

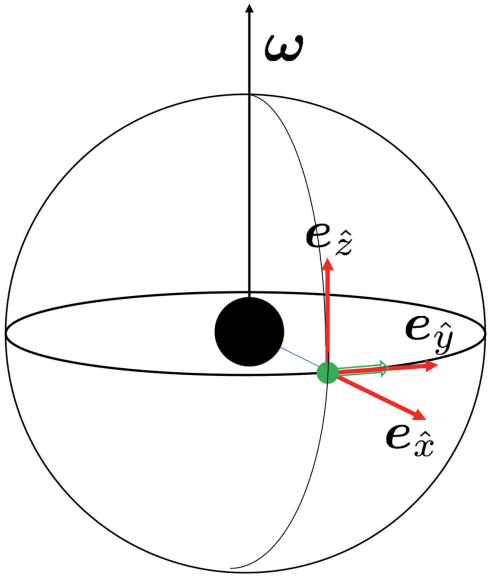

FIG. 1. A local inertial tetrad system $\{\boldsymbol{e}_{\hat{x}}, \boldsymbol{e}_{\hat{y}}, \boldsymbol{e}_{\hat{z}}\}$ rotating with angular frequency $\mathfrak{w}_{\mathrm{R}}$ along a circular orbit.

$$e^{\bar{0}}{}_0 = \sqrt{f(\mathfrak{r}_0)}, \quad e^{\bar{r}}{}_r = \frac{1}{\sqrt{f(\mathfrak{r}_0)}}, \quad e^{\bar{\theta}}{}_{\theta} = \mathfrak{r}_0, \quad e^{\bar{\phi}}{}_{\phi} = \mathfrak{r}_0,$$

the nontrivial components of the Riemann curvature of the Schwarzschild spacetime are given by

$$\bar{\mathcal{R}}_{\bar{0}\bar{r}\bar{0}\bar{r}} = -\frac{\mathfrak{r}_g}{\mathfrak{r}_0^3}, \qquad \bar{\mathcal{R}}_{\bar{0}\bar{\theta}\bar{0}\bar{\theta}} = \bar{\mathcal{R}}_{\bar{0}\bar{\phi}\bar{0}\bar{\phi}} = \frac{\mathfrak{r}_g}{2\mathfrak{r}_0^3},$$
$$\bar{\mathcal{R}}_{\bar{\theta}\bar{\phi}\bar{\theta}\bar{\phi}} = \frac{\mathfrak{r}_g}{\mathfrak{r}_0^3}, \qquad \bar{\mathcal{R}}_{\bar{r}\bar{\theta}\bar{r}\bar{\theta}} = R_{\bar{r}\bar{\phi}\bar{r}\bar{\phi}} = -\frac{\mathfrak{r}_g}{2\mathfrak{r}_0^3}.$$

We then introduce the Descartes coordinates $(\bar{x}, \bar{y}, \bar{z})$ such that $\bar{x}$-direction is the same as the r-direction, but the $\bar{y}$ and $\bar{z}$-directions are ϕ and $-\theta$-directions, respectively, as shown in Fig. 1. Since the tetrad system in this coordinate is given by

$$e^{\bar{0}}{}_0 = \sqrt{f(\mathfrak{r}_0)}, \quad e^{\bar{x}}{}_r = \frac{1}{\sqrt{f(\mathfrak{r}_0)}}, \quad e^{\bar{y}}{}_{\phi} = \mathfrak{r}_0, \quad e^{\bar{z}}{}_{\theta} = -\mathfrak{r}_0,$$

we find the curvature components in this tetrad system as

$$\bar{\mathcal{R}}_{\bar{0}\bar{x}\bar{0}\bar{x}} = -\frac{\mathfrak{r}_g}{\mathfrak{r}_0^3}, \qquad \bar{\mathcal{R}}_{\bar{0}\bar{y}\bar{0}\bar{y}} = \bar{\mathcal{R}}_{\bar{0}\bar{z}\bar{0}\bar{z}} = \frac{\mathfrak{r}_g}{2\mathfrak{r}_0^3},$$
$$\bar{\mathcal{R}}_{\bar{y}\bar{z}\bar{y}\bar{z}} = \frac{\mathfrak{r}_g}{\mathfrak{r}_0^3}, \qquad R_{\bar{x}\bar{y}\bar{x}\bar{y}} = \bar{\mathcal{R}}_{\bar{z}\bar{x}\bar{z}\bar{x}} = -\frac{\mathfrak{r}_g}{2\mathfrak{r}_0^3}.$$

The transformation matrix between the observer's tetrad and static tetrad $(\bar{x}, \bar{y}, \bar{z})$ is given by

$$\Lambda_0{}^{\bar{\alpha}} = \left(\sqrt{1+\mathfrak{r}_0^2\mathfrak{w}_0^2}, 0, \mathfrak{r}_0\mathfrak{w}_0, 0\right),$$
$$\Lambda_{\hat{1}}{}^{\bar{\alpha}} = (0,1,0,0),$$
$$\Lambda_{\hat{2}}{}^{\bar{\alpha}} = \left(\mathfrak{r}_0\mathfrak{w}_0, 0, \sqrt{1+\mathfrak{r}_0^2\mathfrak{w}_0^2}, 0\right),$$
$$\Lambda_{\hat{3}}{}^{\bar{\alpha}} = (0,0,0,1).$$

It is just the Lorentz boost with velocity

$$\mathfrak{v} = \frac{\mathfrak{r}_0\mathfrak{w}_0}{\sqrt{1+\mathfrak{r}_0^2\mathfrak{w}_0^2}},$$

in 0-y plane.

The components in the observer's proper reference frame are given by

$$\bar{\mathcal{R}}_{\hat{0}\hat{x}\hat{0}\hat{x}} = -\bar{\mathcal{R}}_{\hat{y}\hat{z}\hat{y}\hat{z}} = -\left(1+\frac{3}{2}\mathfrak{r}_0^2\mathfrak{w}_0^2\right)\frac{\mathfrak{r}_g}{\mathfrak{r}_0^3},$$
$$\bar{\mathcal{R}}_{\hat{0}\hat{y}\hat{0}\hat{y}} = -\bar{\mathcal{R}}_{\hat{z}\hat{x}\hat{z}\hat{x}} = \frac{1}{2}\frac{\mathfrak{r}_g}{\mathfrak{r}_0^3},$$
$$\bar{\mathcal{R}}_{\hat{0}\hat{z}\hat{0}\hat{z}} = -\bar{\mathcal{R}}_{\hat{x}\hat{y}\hat{x}\hat{y}} = \left(\frac{1+3\mathfrak{r}_0^2\mathfrak{w}_0^2}{2}\right)\frac{\mathfrak{r}_g}{\mathfrak{r}_0^3},$$
$$\bar{\mathcal{R}}_{\hat{0}\hat{x}\hat{y}\hat{x}} = -\bar{\mathcal{R}}_{\hat{0}\hat{z}\hat{y}\hat{z}} = -\frac{3}{2}\epsilon_1\mathfrak{r}_0\mathfrak{w}_0\sqrt{1+\mathfrak{r}_0^2\mathfrak{w}_0^2}\,\frac{\mathfrak{r}_g}{\mathfrak{r}_0^3}.$$

B. Equations of motion of a binary

Since the CM of a binary follows the observer's circular geodesic ($\boldsymbol{R}=0$), we have to solve only the equations of motion for the relative coordinate $\boldsymbol{r}$. Using $x = r^{\hat{1}}, y = r^{\hat{2}}, z = r^{\hat{3}}$, the relative motion of a binary is given by the Lagrangian

$$\mathcal{L}_{\rm rel}(\boldsymbol{r},\dot{\boldsymbol{r}}) = \frac{1}{2}\mu\dot{\boldsymbol{r}}^2 + \frac{Gm_1m_2}{r} + \mathcal{L}_{\text{rel-}\mathfrak{w}}(\boldsymbol{r},\dot{\boldsymbol{r}}) + \mathcal{L}_{\text{rel-}\bar{\mathcal{R}}}(\boldsymbol{r},\dot{\boldsymbol{r}}), \tag{4.6}$$

with

$$\mathcal{L}_{\text{rel-}\mathfrak{w}} = -\mu\left[\mathfrak{w}_0(x\dot{y}-y\dot{x}) - \frac{\mathfrak{w}_0^2}{2}(x^2+y^2)\right],$$
$$\mathcal{L}_{\text{rel-}\bar{\mathcal{R}}} = -\frac{\mu}{2}(\bar{\mathcal{R}}_{\hat{0}\hat{x}\hat{0}\hat{x}}x^2 + \bar{\mathcal{R}}_{\hat{0}\hat{y}\hat{0}\hat{y}}y^2 + \bar{\mathcal{R}}_{\hat{0}\hat{z}\hat{0}\hat{z}}z^2)$$
$$= -\frac{\mu\mathfrak{r}_g}{4\mathfrak{r}_0^3}\left[y^2 - 2x^2 + z^2 + 3\mathfrak{r}_0^2\mathfrak{w}_0^2(-x^2+z^2)\right].$$

The first and second terms in rel-$\mathfrak{w}$ describe the Coriolis force and the centrifugal force, respectively. The first half terms in $\mathcal{L}_{\text{rel-}\bar{\mathcal{R}}}$ are the same as those in Newtonian hierarchical triple system under quadrupole approximation, while the last half terms are relativistic corrections. Note that in the present approach (approximation up to the second order of $x^{\hat{a}}$), we cannot go beyond quadrupole approximation.

In order to analyze the relative motion of a binary, it may be better to go to a nonrotating initial reference frame. Since the angular frequency of a rotating tetrad frame is $\mathfrak{w}_{\rm R}$, the position (x,y,z) in the rotating frame can be replaced by the position $(\mathsf{x},\mathsf{y},\mathsf{z})$ in a nonrotating Descartes' coordinate system by use of the following transformation:

$$x = \mathsf{x}\cos\mathfrak{w}_{\rm R}\tau - \mathsf{y}\sin\mathfrak{w}_{\rm R}\tau,$$
$$y = \mathsf{x}\sin\mathfrak{w}_{\rm R}\tau + \mathsf{y}\cos\mathfrak{w}_{\rm R}\tau,$$
$$z = \mathsf{z}.$$

The Lagrangian $\mathcal{L}_{\rm rel}$ in a nonrotating proper reference frame is given by

$$\mathcal{L}_{\rm rel} = \frac{1}{2}\mu\left(\frac{d\mathbf{r}}{d\tau}\right)^2 + \frac{Gm_1m_2}{\mathsf{r}} + \mathcal{L}_{\text{rel}-dS}(\mathbf{r},\dot{\mathbf{r}}) + \mathcal{L}_{\text{rel-}\bar{\mathcal{R}}}(\mathbf{r},\tau), \tag{4.7}$$

where

$$\mathcal{L}_{\text{rel-dS}}(\mathbf{r},\dot{\mathbf{r}}) = \mu\mathfrak{w}_{\rm dS}(\dot{\mathsf{x}}\mathsf{y}-\dot{\mathsf{y}}\mathsf{x}) + \frac{\mu}{2}\mathfrak{w}_{\rm dS}^2(\mathsf{x}^2+\mathsf{y}^2),$$
$$\mathcal{L}_{\text{rel-}\bar{\mathcal{R}}}(\mathbf{r},\tau) = -\frac{\mu\mathfrak{r}_g}{4\mathfrak{r}_0^3}\Big[\mathsf{x}^2+\mathsf{y}^2+\mathsf{z}^2 - 3(1+\mathfrak{r}_0^2\mathfrak{w}_0^2)$$
$$(\mathsf{x}\cos\mathfrak{w}_{\rm R}\tau - \mathsf{y}\sin\mathfrak{w}_{\rm R}\tau)^2 + 3\mathfrak{r}_0^2\mathfrak{w}_0^2\mathsf{z}^2\Big].$$

Since the momentum is defined by

$$\mathsf{p}_{\mathsf{x}} \equiv \frac{\partial\mathcal{L}}{\partial\dot{\mathsf{x}}} = \mu\dot{\mathsf{x}} + \mu\mathfrak{w}_{\rm dS}\mathsf{y},$$
$$\mathsf{p}_{\mathsf{y}} \equiv \frac{\partial\mathcal{L}}{\partial\dot{\mathsf{y}}} = \mu\dot{\mathsf{y}} - \mu\mathfrak{w}_{\rm dS}\mathsf{x},$$
$$\mathsf{p}_{\mathsf{z}} \equiv \frac{\partial\mathcal{L}}{\partial\dot{\mathsf{z}}} = \mu\dot{\mathsf{z}},$$

we obtain the Hamiltonian as

$$\mathcal{H}_{\rm rel} = \mathcal{H}_0 + \mathcal{H}_1, \tag{4.8}$$

where

$$\mathcal{H}_0 = \frac{1}{2\mu}\mathbf{p}^2 - \frac{Gm_1m_2}{\mathsf{r}},$$
$$\mathcal{H}_1 = \mathcal{H}_{\text{1-dS}} + \mathcal{H}_{\text{1-}\bar{\mathcal{R}}},$$

with

$$\mathcal{H}_{\text{1-dS}} = \mathfrak{w}_{\rm dS}(\mathsf{p}_{\mathsf{y}}\mathsf{x} - \mathsf{p}_{\mathsf{x}}\mathsf{y}),$$
$$\mathcal{H}_{\text{1}-\bar{\mathcal{R}}} = \frac{\mu\mathfrak{r}_g}{4\mathfrak{r}_0^3}\Big[\mathsf{x}^2+\mathsf{y}^2+\mathsf{z}^2 - 3(1+\mathfrak{r}_0^2\mathfrak{w}_0^2)$$
$$(\mathsf{x}\cos\mathfrak{w}_{\rm R}\tau - \mathsf{y}\sin\mathfrak{w}_{\rm R}\tau)^2 + 3\mathfrak{r}_0^2\mathfrak{w}_0^2\mathsf{z}^2\Big].$$

The term $\mathcal{H}_{\text{1-dS}}$ gives the so-called de Sitter precession as follows. Let us consider the model with $\mathcal{H}' = \mathcal{H}_0 + \mathcal{H}_{\text{1-dS}}$. The Hamilton equations are given as

$$\dot{\mathsf{x}} = \frac{\partial \mathcal{H}'}{\partial \mathsf{p}_\mathsf{x}} = \frac{\mathsf{p}_\mathsf{x}}{\mu} - \mathfrak{w}_{\mathrm{dS}}\mathsf{y},$$
$$\dot{\mathsf{y}} = \frac{\partial \mathcal{H}'}{\partial \mathsf{p}_\mathsf{y}} = \frac{\mathsf{p}_\mathsf{y}}{\mu} + \mathfrak{w}_{\mathrm{dS}}\mathsf{x},$$
$$\dot{\mathsf{z}} = \frac{\partial \mathcal{H}'}{\partial \mathsf{p}_\mathsf{z}} = \frac{\mathsf{p}_z}{\mu},$$

and

$$\dot{\mathsf{p}}_\mathsf{x} = -\frac{\partial \mathcal{H}'}{\partial \mathsf{x}} = -\frac{Gm_1m_2\mathsf{x}}{\mathsf{r}^3} - \mathfrak{w}_{\mathrm{dS}}\mathsf{p}_\mathsf{y},$$
$$\dot{\mathsf{p}}_\mathsf{y} = -\frac{\partial \mathcal{H}'}{\partial \mathsf{y}} = -\frac{Gm_1m_2\mathsf{y}}{\mathsf{r}^3} + \mathfrak{w}_{\mathrm{dS}}\mathsf{p}_\mathsf{x},$$
$$\dot{\mathsf{p}}_\mathsf{z} = -\frac{\partial \mathcal{H}'}{\partial \mathsf{z}} = -\frac{Gm_1m_2\mathsf{z}}{\mathsf{r}^3}.$$

We then calculate the time evolution of the angular momentum $\boldsymbol{L} = (L_\mathsf{x}, L_\mathsf{y}, L_\mathsf{z})$. Using the equations of motion, we find

$$\dot{L}_\mathsf{x} = \frac{d}{d\tau}(\mathsf{y}\mathsf{p}_\mathsf{z} - \mathsf{z}\mathsf{p}_\mathsf{y}) = \dot{\mathsf{y}}\mathsf{p}_\mathsf{z} + \mathsf{y}\dot{\mathsf{p}}_\mathsf{z} - \dot{\mathsf{z}}\mathsf{p}_\mathsf{y} - \mathsf{z}\dot{\mathsf{p}}_\mathsf{y} = -\mathfrak{w}_{\mathrm{dS}}L_\mathsf{y},$$
$$\dot{L}_\mathsf{y} = \frac{d}{d\tau}(\mathsf{z}\mathsf{p}_\mathsf{x} - \mathsf{x}\mathsf{p}_\mathsf{z}) = \dot{\mathsf{z}}\mathsf{p}_\mathsf{x} + \mathsf{z}\dot{\mathsf{p}}_\mathsf{x} - \dot{\mathsf{x}}\mathsf{p}_\mathsf{z} - \mathsf{x}\dot{\mathsf{p}}_\mathsf{z} = \mathfrak{w}_{\mathrm{dS}}L_\mathsf{x},$$
$$\dot{L}_\mathsf{z} = \frac{d}{d\tau}(\mathsf{x}\mathsf{p}_\mathsf{y} - \mathsf{y}\mathsf{p}_\mathsf{x}) = \dot{\mathsf{x}}\mathsf{p}_\mathsf{y} + \mathsf{x}\dot{\mathsf{p}}_\mathsf{y} - \dot{\mathsf{y}}\mathsf{p}_\mathsf{x} - \mathsf{y}\dot{\mathsf{p}}_\mathsf{x} = 0.$$

From these equations, we find that the z-component of the angular momentum is conserved, and $(L_\mathsf{x}, L_\mathsf{y})$ rotates around the z-axis with the constant angular frequency $\mathfrak{w}_{\mathrm{dS}}$ which is just the de Sitter precession. The full equations are given as

$$\dot{\mathsf{x}} = \frac{\partial \mathcal{H}}{\partial \mathsf{p}_\mathsf{x}} = \frac{\mathsf{p}_\mathsf{x}}{\mu} - \mathfrak{w}_{\mathrm{dS}}\mathsf{y}, \tag{4.9}$$
$$\dot{\mathsf{y}} = \frac{\partial \mathcal{H}}{\partial \mathsf{p}_\mathsf{y}} = \frac{\mathsf{p}_\mathsf{y}}{\mu} + \mathfrak{w}_{\mathrm{dS}}\mathsf{x}, \tag{4.10}$$
$$\dot{\mathsf{z}} = \frac{\partial \mathcal{H}}{\partial \mathsf{p}_\mathsf{z}} = \frac{\mathsf{p}_\mathsf{z}}{\mu}, \tag{4.11}$$

and

$$\dot{\mathsf{p}}_\mathsf{x} = -\frac{\partial \mathcal{H}}{\partial \mathsf{x}} = -\frac{Gm_1m_2}{\mathsf{r}^3}\mathsf{x} - \mathfrak{w}_{\mathrm{dS}}\mathsf{p}_\mathsf{y} - \frac{\mu\mathfrak{r}_g}{2\mathfrak{r}_0^3}\{\mathsf{x} - 3(1+\mathfrak{r}_0^2\mathfrak{w}_0^2)(\mathsf{x}\cos\mathfrak{w}_\mathrm{R}\tau - \mathsf{y}\sin\mathfrak{w}_\mathrm{R}\tau)\cos\mathfrak{w}_\mathrm{R}\tau\}, \tag{4.12}$$

$$\dot{\mathsf{p}}_\mathsf{y} = -\frac{\partial \mathcal{H}}{\partial \mathsf{y}} = -\frac{Gm_1m_2}{\mathsf{r}^3}\mathsf{y} + \mathfrak{w}_{\mathrm{dS}}\mathsf{p}_\mathsf{x} - \frac{\mu\mathfrak{r}_g}{2\mathfrak{r}_0^3}\{\mathsf{y} + 3(1+\mathfrak{r}_0^2\mathfrak{w}_0^2)(\mathsf{x}\cos\mathfrak{w}_\mathrm{R}\tau - \mathsf{y}\sin\mathfrak{w}_\mathrm{R}\tau)\sin\mathfrak{w}_\mathrm{R}\tau\}, \tag{4.13}$$

$$\dot{\mathsf{p}}_\mathsf{z} = -\frac{\partial \mathcal{H}}{\partial \mathsf{z}} = -\frac{Gm_1m_2}{\mathsf{r}^3}\mathsf{z} - \frac{\mu\mathfrak{r}_g}{2\mathfrak{r}_0^3}(1+3\mathfrak{r}_0^2\mathfrak{w}_0^2)\mathsf{z}. \tag{4.14}$$

C. Motion with 0.5 PN correction term

Now we consider 0.5 PN terms. As discussed in Sec. III, we can assume $\boldsymbol{R} = 0$ by introduction of the acceleration given by Eq. (3.9). We first solve the relative coordinates $\boldsymbol{r}$, and then the motion of the observer (or the CM).

1. Equations of motion for relative coordinates

The equation of motion for relative coordinates $\boldsymbol{r}$ of a binary is now given by

$$\tilde{\mathcal{L}}_{\mathrm{rel}}(\boldsymbol{r}, \dot{\boldsymbol{r}}) = \mathcal{L}_{\mathrm{rel}}(\boldsymbol{r}, \dot{\boldsymbol{r}}) + \mathcal{L}_{1/2\text{-rel}}(\boldsymbol{r}, \dot{\boldsymbol{r}}),$$

where $\mathcal{L}_{\mathrm{rel}}$ is given by Eq. (4.6), while

$$\begin{aligned}\mathcal{L}_{1/2\text{-rel}}(\boldsymbol{r}, \dot{\boldsymbol{r}}) &= -\mu\frac{2(m_1-m_2)}{3(m_1+m_2)}(\bar{\mathcal{R}}_{\hat{0}\hat{x}\hat{y}\hat{x}}x(x\dot{y}-y\dot{x}) + \bar{\mathcal{R}}_{\hat{0}\hat{z}\hat{y}\hat{z}}z(z\dot{y}-y\dot{z})) \\ &= -\mu\frac{\mathfrak{r}_g}{\mathfrak{r}_0^3}\frac{m_1-m_2}{m_1+m_2}\mathfrak{r}_0\mathfrak{w}_0\sqrt{1+\mathfrak{r}_0^2\mathfrak{w}_0^2}(-x(x\dot{y}-y\dot{x}) + z(z\dot{y}-y\dot{z})).\end{aligned}$$

In nonrotating Fermi-Walker coordinates, we find $\mathcal{L}_{\rm rel}$ is given by Eq. (4.7), while

$$\mathcal{L}_{1/2\text{-rel}}(\boldsymbol{r},\dot{\boldsymbol{r}}) = \mu\frac{\mathfrak{r}_g}{\mathfrak{r}_0^3}\frac{m_1-m_2}{m_1+m_2}\mathfrak{r}_0\mathfrak{w}_0\sqrt{1+\mathfrak{r}_0^2\mathfrak{w}_0^2}\Big\{\cos\mathfrak{w}_{\rm R}\tau[\mathsf{x}(\mathsf{x}\dot{\mathsf{y}}-\mathsf{y}\dot{\mathsf{x}})+\mathsf{z}(\mathsf{y}\dot{\mathsf{z}}-\mathsf{z}\dot{\mathsf{y}})+\mathfrak{w}_{\rm R}\mathsf{x}(\mathsf{x}^2+\mathsf{y}^2-\mathsf{z}^2)] - \sin\mathfrak{w}_{\rm R}\tau[\mathsf{y}(\mathsf{x}\dot{\mathsf{y}}-\mathsf{y}\dot{\mathsf{x}})+\mathsf{z}(\mathsf{z}\dot{\mathsf{x}}-\mathsf{x}\dot{\mathsf{z}})+\mathfrak{w}_{\rm R}\mathsf{y}(\mathsf{x}^2+\mathsf{y}^2-\mathsf{z}^2)]\Big\}.$$

The momentum is obtained from the Lagrangian $\tilde{\mathcal{L}}_{\rm rel}(\mathbf{r},\dot{\mathbf{r}})$ as

$$p_{\mathsf{x}} = \mu\dot{\mathsf{x}}+\mu\mathfrak{w}_{\rm dS}\mathsf{y}+\mu\frac{\mathfrak{r}_g}{\mathfrak{r}_0^3}\frac{m_1-m_2}{m_1+m_2}\mathfrak{r}_0\mathfrak{w}_0\sqrt{1+\mathfrak{r}_0^2\mathfrak{w}_0^2}(-\mathsf{x}\mathsf{y}\cos\mathfrak{w}_{\rm R}\tau+(\mathsf{y}^2-\mathsf{z}^2)\sin\mathfrak{w}_{\rm R}\tau),$$
$$p_{\mathsf{y}} = \mu\dot{\mathsf{y}}-\mu\mathfrak{w}_{\rm dS}\mathsf{x}+\mu\frac{\mathfrak{r}_g}{\mathfrak{r}_0^3}\frac{m_1-m_2}{m_1+m_2}\mathfrak{r}_0\mathfrak{w}_0\sqrt{1+\mathfrak{r}_0^2\mathfrak{w}_0^2}(-\mathsf{x}\mathsf{y}\sin\mathfrak{w}_{\rm R}\tau+(\mathsf{x}^2-\mathsf{z}^2)\cos\mathfrak{w}_{\rm R}\tau),$$
$$p_{\mathsf{z}} = \mu\dot{\mathsf{z}}+\mu\frac{\mathfrak{r}_g}{\mathfrak{r}_0^3}\frac{m_1-m_2}{m_1+m_2}\mathfrak{r}_0\mathfrak{w}_0\sqrt{1+\mathfrak{r}_0^2\mathfrak{w}_0^2}\mathsf{z}(\mathsf{y}\cos\mathfrak{w}_{\rm R}\tau+\mathsf{x}\sin\mathfrak{w}_{\rm R}\tau).$$

The Hamiltonian is given by

$$\tilde{\mathcal{H}}_{\rm rel}(\mathbf{r},\mathbf{p}) = \mathcal{H}_{\rm rel}(\mathbf{r},\mathbf{p})+\mathcal{H}_{1/2\text{-rel}}(\mathbf{r},\mathbf{p}),$$

where $\mathcal{H}_{\rm rel}(\mathbf{r},\mathbf{p})$ is given by Eq. (4.8), while

$$\mathcal{H}_{1/2\text{-rel}}(\mathbf{r},\mathbf{p}) = -\frac{1}{2}\mu\left(\frac{\mathfrak{r}_g}{\mathfrak{r}_0^3}\right)^2\frac{(m_1-m_2)^2}{(m_1+m_2)^2}\mathfrak{r}_0^2\mathfrak{w}_0^2(1+\mathfrak{r}_0^2\mathfrak{w}_0^2)\Big[(-\mathsf{x}\mathsf{y}\cos\mathfrak{w}_{\rm R}\tau+(\mathsf{y}^2-\mathsf{z}^2)\sin\mathfrak{w}_{\rm R}\tau)^2 + (-\mathsf{x}\mathsf{y}\sin\mathfrak{w}_{\rm R}\tau+(\mathsf{x}^2-\mathsf{z}^2)\cos\mathfrak{w}_{\rm R}\tau)^2+\mathsf{z}^2(\mathsf{y}\cos\mathfrak{w}_{\rm R}\tau+\mathsf{x}\sin\mathfrak{w}_{\rm R}\tau)^2\Big].$$

This Hamiltonian is very complicated, but it should be ignored because it is beyond quadrupole approximation, although momentum is modified. For an equal mass binary ($m_1 = m_2$), the 0.5 PN correction term vanishes and the momentum is also the same as the Newtonian one. As a result, the Newtonian solution is also a solution.

2. Motion of the CM of a binary and its stability

In order to study stability of the CM of a binary system, we analyze Eq. (3.9). Since $\boldsymbol{R}$ is measured by the circular observer at $\mathfrak{r} = \mathfrak{r}_0$, we can split the 4-velocity u^μ as

$$u^\mu = u^\mu_{(0)}+u^\mu_{(1)},$$

where

$$u^\mu_{(0)} = \frac{d\mathfrak{x}^\mu_{(0)}}{d\tau} = (u^0_{(0)},0,0,u^3_{(0)}) = \left(\sqrt{\frac{1+\mathfrak{r}_0^2\mathfrak{w}_0^2}{f(\mathfrak{r}_0)}},0,0,\mathfrak{w}_0\right),$$
$$u^\mu_{(1)} = \frac{d\mathfrak{x}^\mu_{(1)}}{d\tau},$$

with

$$\mathfrak{x}^\mu_{(0)} = \left(\sqrt{\frac{1+\mathfrak{r}_0^2\mathfrak{w}_0^2}{f(\mathfrak{r}_0)}}\tau,\mathfrak{r}_0,\frac{\pi}{2},\mathfrak{w}_0\tau\right),$$
$$\mathfrak{x}^\mu_{(1)} \equiv e^\mu{}_{\hat{\ell}}R^{\hat{\ell}}.$$

The acceleration a^μ is given by the motion of a binary $x^{\hat{\mu}}(\tau)$ in a rotating frame as

$$a^\mu = -\frac{3\mu}{m_1+m_2}\mathfrak{w}_0\sqrt{1+\mathfrak{r}_0^2\mathfrak{w}_0^2}\frac{\mathfrak{r}_g}{\mathfrak{r}_0^2}\left[\left(\delta_0^\mu\frac{\mathfrak{r}_0\mathfrak{w}_0}{\sqrt{f(\mathfrak{r}_0)}}+\delta_3^\mu\frac{\sqrt{1+\mathfrak{r}_0^2\mathfrak{w}_0^2}}{\mathfrak{r}_0}\right)(\dot{x}x-\dot{z}z)-\delta_1^\mu\sqrt{f(\mathfrak{r}_0)}\dot{y}x-\delta_2^\mu\frac{1}{\mathfrak{r}_0}\dot{y}z\right].$$

Here we assume that the deviation from a circular orbit is small, i.e., $\mathfrak{x}^\mu_{(1)}$ and $u^\mu_{(1)}$ are small perturbations. Ignoring nonlinear deviation terms in the equations of motion $\frac{Du^\mu}{d\tau}=a^\mu$, because the circular orbit $\mathfrak{x}^\mu_{(0)}(\tau)$ is a geodesic, we obtain a linear differential equation as

$$\frac{du^\mu_{(1)}}{d\tau}+2\Gamma^\mu{}_{\rho\sigma}(\mathfrak{r}_0)u^\rho_{(0)}u^\sigma_{(1)}+\frac{\partial\Gamma^\mu_{\rho\sigma}}{\partial\mathfrak{x}^\alpha}(\mathfrak{r}_0)\mathfrak{x}^\alpha_{(1)}u^\rho_{(0)}u^\sigma_{(0)}=a^\mu,$$

where a^μ acts as an external force. Describing the deviation as

$$\mathfrak{x}^\mu_{(1)}=(\mathfrak{t}_{(1)},\mathfrak{r}_{(1)},\theta_{(1)},\varphi_{(1)}),$$

we find

$$\frac{d^2\mathfrak{t}_{(1)}}{d\tau^2}+\frac{\mathfrak{r}_g}{\mathfrak{r}_0^2f(\mathfrak{r}_0)}\sqrt{\frac{1+\mathfrak{r}_0^2\mathfrak{w}^2}{f(\mathfrak{r}_0)}}\frac{d\mathfrak{r}_{(1)}}{d\tau}=a^0=-\frac{3\mu}{m_1+m_2}\frac{\mathfrak{w}_0^2\mathfrak{r}_g}{\mathfrak{r}_0}\sqrt{\frac{1+\mathfrak{r}_0^2\mathfrak{w}_0^2}{f(\mathfrak{r}_0)}}(\dot{x}x-\dot{z}z), \tag{4.15}$$

$$\begin{aligned}&\frac{d^2\mathfrak{r}_{(1)}}{d\tau^2}-\frac{3\mathfrak{r}_g}{2\mathfrak{r}_0^3}(1+\mathfrak{r}_0^2\mathfrak{w}_0^2)\mathfrak{r}_{(1)}+\frac{\mathfrak{r}_g}{\mathfrak{r}_0^2}f(\mathfrak{r}_0)\sqrt{\frac{1+\mathfrak{r}_0^2\mathfrak{w}^2}{f(\mathfrak{r}_0)}}\frac{d\mathfrak{t}_{(1)}}{d\tau}-2\mathfrak{r}_0\mathfrak{w}_0f(\mathfrak{r}_0)\frac{d\varphi_{(1)}}{d\tau}\\&=a^1=\frac{3\mu}{m_1+m_2}\frac{\mathfrak{w}_0\mathfrak{r}_g}{\mathfrak{r}_0^2}\sqrt{f(\mathfrak{r}_0)(1+\mathfrak{r}_0^2\mathfrak{w}_0^2)}\dot{y}x,\end{aligned} \tag{4.16}$$

$$\frac{d^2\theta_{(1)}}{d\tau^2}+\mathfrak{w}_0^2\theta_{(1)}=a^2=\frac{3\mu}{m_1+m_2}\frac{\mathfrak{w}_0\mathfrak{r}_g}{\mathfrak{r}_0^3}\sqrt{1+\mathfrak{r}_0^2\mathfrak{w}_0^2}\dot{y}z, \tag{4.17}$$

$$\frac{d^2\varphi_{(1)}}{d\tau^2}+2\frac{\mathfrak{w}_0}{\mathfrak{r}_0}\frac{d\mathfrak{r}_{(1)}}{d\tau}=a^3=-\frac{3\mu}{m_1+m_2}\frac{\mathfrak{w}_0\mathfrak{r}_g}{\mathfrak{r}_0^3}(1+\mathfrak{r}_0^2\mathfrak{w}_0^2)(\dot{x}x-\dot{z}z). \tag{4.18}$$

Integrating Eqs. (4.15) and (4.18), we obtain

$$\frac{d\mathfrak{t}_{(1)}}{d\tau}=-\frac{\mathfrak{r}_g}{\mathfrak{r}_0^2f(\mathfrak{r}_0)}\sqrt{\frac{1+\mathfrak{r}_0^2\mathfrak{w}_0^2}{f(\mathfrak{r}_0)}}\mathfrak{r}_{(1)}-\frac{3\mu}{2(m_1+m_2)}\frac{\mathfrak{w}_0^2\mathfrak{r}_g}{\mathfrak{r}_0}\sqrt{\frac{1+\mathfrak{r}_0^2\mathfrak{w}_0^2}{f(\mathfrak{r}_0)}}(x^2-z^2), \tag{4.19}$$

$$\frac{d\varphi_{(1)}}{d\tau}=-2\frac{\mathfrak{w}_0}{\mathfrak{r}_0}\mathfrak{r}_{(1)}-\frac{3\mu}{2(m_1+m_2)}\frac{\mathfrak{w}_0\mathfrak{r}_g}{\mathfrak{r}_0^3}(1+\mathfrak{r}_0^2\mathfrak{w}_0^2)(x^2-z^2), \tag{4.20}$$

where we set the integration constants at zero. Plugging Eqs. (4.19) and (4.20) into Eq. (4.16) with Eq. (4.3), we obtain the perturbation equation for the radial coordinates $\mathfrak{r}_{(1)}$ as

$$\frac{d^2\mathfrak{r}_{(1)}}{d\tau^2}+k^2\mathfrak{r}_{(1)}+A(x^2-z^2)+B\dot{y}x=0, \tag{4.21}$$

where

$$k^2=\frac{\mathfrak{r}_g(\mathfrak{r}_0-3\mathfrak{r}_g)}{\mathfrak{r}_0^3(2\mathfrak{r}_0-3\mathfrak{r}_g)}, \tag{4.22}$$

$$A = \frac{3\mu}{m_1+m_2}\frac{\mathfrak{r}_g^2(\mathfrak{r}_0-\mathfrak{r}_g)}{\mathfrak{r}_0^5(2\mathfrak{r}_0-3\mathfrak{r}_g)} \tag{4.23}$$

$$B = -\frac{3\mu}{m_1+m_2}\sqrt{\frac{2\mathfrak{r}_g^3}{\mathfrak{r}_0^7}}\frac{(\mathfrak{r}_0-\mathfrak{r}_g)}{(2\mathfrak{r}_0-3\mathfrak{r}_g)}. \tag{4.24}$$

We find that $k^2 > 0$ when $\mathfrak{r}_0 > 3\mathfrak{r}_g$, while $A > 0$ and $B < 0$ when $\mathfrak{r}_0 > 3\mathfrak{r}_g/2$. The condition for $k^2 > 0$ is consistent with the fact that the radius of the innermost stable circular orbit (ISCO) is $3\mathfrak{r}_g$.

If the binary orbit is bounded [$x(\tau)$, $y(\tau)$, and $z(\tau)$ are finite], the orbit of the center of mass is also bounded because $k^2 > 0$. We expect that when $\mathfrak{r}_0 > 3\mathfrak{r}_g$ (ISCO radius), a binary system near SMBH is linearly stable unless a binary is broken.

V. NUMERICAL ANALYSIS

A. Validity and stability

Before showing our numerical results, we discuss the validity of the present approach. The minimum curvature radius at the radius $\mathfrak{r}_0$ is evaluated as

$$\begin{aligned}\ell_{\bar{\mathcal{R}}} &= \min\left[|\bar{\mathcal{R}}_{\hat{\mu}\hat{\nu}\hat{\rho}\hat{\sigma}}|^{-\frac{1}{2}}, |\bar{\mathcal{R}}_{\hat{\mu}\hat{\nu}\hat{\rho}\hat{\sigma};\hat{\alpha}}|^{-\frac{1}{3}}, |\bar{\mathcal{R}}_{\hat{\mu}\hat{\nu}\hat{\rho}\hat{\sigma};\hat{\alpha};\hat{\beta}}|^{-\frac{1}{4}}\right]\\ &\sim \min\left[\left(\frac{\mathfrak{r}_g}{\mathfrak{r}_0^3}\right)^{-\frac{1}{2}}, \left(\frac{\mathfrak{r}_g}{\mathfrak{r}_0^4}\right)^{-\frac{1}{3}}, \left(\frac{\mathfrak{r}_g}{\mathfrak{r}_0^5}\right)^{-\frac{1}{4}}\right]\\ &\sim \mathfrak{r}_0\left(\frac{\mathfrak{r}_0}{\mathfrak{r}_g}\right)^{1/4} \geq 3\sqrt[4]{3}\mathfrak{r}_g \sim 8\ \mathrm{AU}\left(\frac{M}{10^8 M_\odot}\right).\end{aligned}$$

The equality is held at the ISCO radius $\mathfrak{r}_0 = 3\mathfrak{r}_g$.

When we put a binary at $\mathfrak{r} = \mathfrak{r}_0$, the binary size ℓ_{binary} should satisfy

$$\ell_{\mathrm{binary}} \ll \ell_{\bar{\mathcal{R}}}.$$

As for stability of a binary, the mutual gravitational interaction between a binary should be much larger than the tidal force by a third body. The condition is given by

$$\frac{Gm_1m_2}{r^2} \gg \frac{\mu\mathfrak{r}_g}{\mathfrak{r}_0^3}r,$$

which gives the constraint on a binary size ℓ_{binary} as

$$\begin{aligned}\ell_{\mathrm{binary}} &\ll \left(\frac{m_1+m_2}{2M}\right)^{\frac{1}{3}}\mathfrak{r}_0\\ &\approx 4.64\times10^{-3}\left(\frac{(m_1+m_2)}{20M_\odot}\right)^{\frac{1}{3}}\left(\frac{M}{10^8M_\odot}\right)^{-\frac{1}{3}}\mathfrak{r}_0.\end{aligned} \tag{5.1}$$

When we are interested in the orbit near the ISCO radius $\mathfrak{r}_0 = 3\mathfrak{r}_g$, we find

$$\ell_{\mathrm{binary}} \ll 3\times10^{-2}\ \mathrm{AU}\left(\frac{(m_1+m_2)}{20M_\odot}\right)^{\frac{1}{3}}\left(\frac{M}{10^8M_\odot}\right)^{\frac{2}{3}}.$$

We also have another criterion for stability. In order to avoid a chaotic energy exchange instability, we may have to impose the condition for the ratio of the circular radius $\mathfrak{r}_0$ to the binary size ℓ_{binary} such that

$$\frac{\mathfrak{r}_0}{\ell_{\mathrm{binary}}} \gtrsim C_{\mathrm{chaotic}}\left(\frac{M}{m_1+m_2}\right)^p$$

when $M \gg m_1, m_2$. Two parameters in this inequality are evaluated by N-body simulations of two groups [62,63] as

$$C_{\mathrm{chaotic}} \sim 2.8 \quad \text{and} \quad p = \frac{2}{5} \quad \text{(criterion 1 by [62])}$$

$$C_{\mathrm{chaotic}} \sim 5.2f^{\frac{1}{3}} \quad \text{and} \quad p = \frac{1}{3} \quad \text{(criterion 2 by [63])}.$$

Although f is a complicated function of inner eccentricity and inclination, it takes the value in the range of 0 to 2.25, but mostly between 0.6 and 1.0.

We should note that the above stability condition is only obtained for stellar masses triples. Therefore, direct N-body integration is a reliable test of stability in such a setting.

Meanwhile, the relativistic effect in a binary becomes important when

$$\begin{aligned}\ell_{\mathrm{binary}} &\leq \frac{G(m_1+m_2)}{c^2}\\ &\approx 2\times10^{-7}\ \mathrm{AU}\left(\frac{(m_1+m_2)}{20M_\odot}\right).\end{aligned}$$

Hence, for a binary with the size of

$$\begin{aligned}&2\times10^{-7}\ \mathrm{AU}\left(\frac{(m_1+m_2)}{20M_\odot}\right) \ll \ell_{\mathrm{binary}}\\ &\ll 3\times10^{-2}\ \mathrm{AU}\left(\frac{(m_1+m_2)}{20M_\odot}\right)^{\frac{1}{3}}\left(\frac{M}{10^8M_\odot}\right)^{\frac{2}{3}},\end{aligned}$$

we may apply the present Newtonian approach to the ISCO radius.

B. Normalization and initial data

Here we show some numerical examples for an equal-mass binary ($m_1 = m_2$). Hence, we have to solve Eqs. (4.9)–(4.14). In order to solve these basic equations, we shall introduce dimensionless variables as follows: The length scale of a binary is normalized by an initial semi-major axis a_0, while the timescale is normalized by an initial binary mean motion n_0, which is defined by

$$n_0 \equiv \left(\frac{G(m_1+m_2)}{a_0^3}\right)^{1/2}.$$

Note that the initial binary period is given by $P_{\rm in} = 2\pi/n_0$. Introducing

$$\tilde{\tau} = n_0\tau,$$
$$\tilde{\mathsf{x}} = \frac{\mathsf{x}}{a_0}, \qquad \tilde{\mathsf{y}} = \frac{\mathsf{y}}{a_0}, \qquad \tilde{\mathsf{z}} = \frac{\mathsf{z}}{a_0}, \qquad \tilde{\mathsf{r}} = \frac{\mathsf{r}}{a_0},$$
$$\tilde{p}_{\mathsf{x}} = \frac{p_{\mathsf{x}}}{\mu a_0 n_0}, \qquad \tilde{p}_{\mathsf{y}} = \frac{p_{\mathsf{y}}}{\mu a_0 n_0}, \qquad \tilde{p}_{\mathsf{z}} = \frac{p_{\mathsf{z}}}{\mu a_0 n_0},$$

we find the dimensionless equations of motion as

$$\frac{d\tilde{\mathsf{x}}}{d\tilde{\tau}} = \tilde{p}_{\mathsf{x}} - \tilde{\mathfrak{w}}_{\rm dS}\tilde{\mathsf{y}}, \tag{5.2}$$

$$\frac{d\tilde{\mathsf{y}}}{d\tilde{\tau}} = \tilde{p}_{\mathsf{y}} + \tilde{\mathfrak{w}}_{\rm dS}\tilde{\mathsf{x}}, \tag{5.3}$$

$$\frac{d\tilde{\mathsf{z}}}{d\tilde{\tau}} = \tilde{p}_{\mathsf{z}}, \tag{5.4}$$

and

$$\frac{d\tilde{\mathsf{p}}_{\mathsf{x}}}{d\tilde{\tau}} = -\frac{\tilde{\mathsf{x}}}{\tilde{\mathsf{r}}^3} - \tilde{\mathfrak{w}}_{\rm dS}\tilde{\mathsf{p}}_{\mathsf{y}} - \frac{\mathfrak{r}_g}{2\mathfrak{r}_0}\epsilon^2\{\tilde{\mathsf{x}} - 3(1+\mathfrak{r}_0^2\mathfrak{w}_0^2) \times (\tilde{\mathsf{x}}\cos\tilde{\mathfrak{w}}_{\rm R}\tilde{\tau} - \tilde{\mathsf{y}}\sin\tilde{\mathfrak{w}}_{\rm R}\tilde{\tau})\cos\tilde{\mathfrak{w}}_{\rm R}\tilde{\tau}\}, \tag{5.5}$$

$$\frac{d\tilde{\mathsf{p}}_{\mathsf{y}}}{d\tilde{\tau}} = -\frac{\tilde{\mathsf{y}}}{\tilde{\mathsf{r}}^3} + \tilde{\mathfrak{w}}_{\rm dS}\tilde{\mathsf{p}}_{\mathsf{x}} - \frac{\mathfrak{r}_g}{2\mathfrak{r}_0}\epsilon^2\{\tilde{\mathsf{y}} + 3(1+\mathfrak{r}_0^2\mathfrak{w}_0^2) \times (\tilde{\mathsf{x}}\cos\tilde{\mathfrak{w}}_{\rm R}\tilde{\tau} - \tilde{\mathsf{y}}\sin\tilde{\mathfrak{w}}_{\rm R}\tilde{\tau})\sin\tilde{\mathfrak{w}}_{\rm R}\tilde{\tau}\}, \tag{5.6}$$

$$\frac{d\tilde{\mathsf{p}}_{\mathsf{z}}}{d\tilde{\tau}} = -\frac{\tilde{\mathsf{z}}}{\tilde{\mathsf{r}}^3} - \frac{\mathfrak{r}_g}{2\mathfrak{r}_0}\epsilon^2(1+3\mathfrak{r}_0^2\mathfrak{w}_0^2)\tilde{\mathsf{z}}, \tag{5.7}$$

where

$$\tilde{\mathfrak{w}}_{\rm dS} \equiv \frac{\mathfrak{w}_{\rm dS}}{n_0}, \qquad \tilde{\mathfrak{w}}_{\rm R} \equiv \frac{\mathfrak{w}_{\rm R}}{n_0},$$
$$\mathfrak{r}_0^2\mathfrak{w}_0^2 = \left(\frac{2\mathfrak{r}_0}{\mathfrak{r}_g} - 3\right)^{-1},$$

and

$$\epsilon^2 \equiv \frac{1}{\mathfrak{r}_0^2 n_0^2} = \left(\frac{a_0}{\mathfrak{r}_0}\right)^3\left(\frac{\mathfrak{r}_0}{\mathfrak{r}_g}\right)\left(\frac{2M}{m_1+m_2}\right). \tag{5.8}$$

This ϵ corresponds to the initial semimajor axis a_0 as

$$a_0 = \epsilon^{\frac{2}{3}}\mathfrak{r}_0\left(\frac{m_1+m_2}{2M}\right)^{1/3}\left(\frac{\mathfrak{r}_0}{\mathfrak{r}_g}\right)^{-1/3}.$$

Using ϵ, we find

$$\tilde{\mathfrak{w}}_{\rm dS} = \epsilon\left[\left(\frac{\mathfrak{r}_g}{2\mathfrak{r}_0 - 3\mathfrak{r}_g}\right)^{\frac{1}{2}} - \left(\frac{\mathfrak{r}_g}{2\mathfrak{r}_0}\right)^{\frac{1}{2}}\right],$$
$$\tilde{\mathfrak{w}}_{\rm R} = \epsilon\left(\frac{\mathfrak{r}_g}{2\mathfrak{r}_0}\right)^{\frac{1}{2}}.$$

As we discuss in Sec. V A, the necessary conditions for a stable "Newtonian" binary is given by the length scale of a binary. If we set $\ell_{\rm binary} \sim a_0$, we find the condition for ϵ as

$$\frac{m_1+m_2}{2M}\left(\frac{\mathfrak{r}_0}{\mathfrak{r}_g}\right)^{-1} \ll \epsilon \lesssim \sqrt{\frac{2\mathfrak{r}_0}{C^3_{\rm chaotic}\mathfrak{r}_g}}\left(\frac{m_1+m_2}{M}\right)^{(3p-1)/2}.$$

When a binary is located near the ISCO radius, this condition is

$$O(10^{-7}) \ll \epsilon \le \epsilon_{\rm chaotic},$$

where $\epsilon_{\rm chaotic}$ is evaluated as $\epsilon_{\rm chaotic} \sim 0.11$ for the criterion 1 by [62] when $m_1 = m_2 = 10M_\odot, M = 10^8 M_\odot$, or $\epsilon_{\rm chaotic} \sim 0.21 f^{-1/2}$ with $f \sim 0.6$–1.0 for the criterion 2 by [63].

In order to solve Eqs. (4.9)–(4.14), we first give masses m_1, m_2, M the radius of the circular orbit $\mathfrak{r}_0$, and ϵ, which corresponds to the initial semimajor axis of a binary a_0. We then provide the initial data of a binary, i.e., $\tilde{\mathsf{x}}(0), \tilde{\mathsf{y}}(0), \tilde{\mathsf{z}}(0)$, and $\tilde{\mathsf{p}}_{\mathsf{x}}(0), \tilde{\mathsf{p}}_{\mathsf{y}}(0), \tilde{\mathsf{p}}_{\mathsf{z}}(0)$.

Since the motion of a binary can be approximated by an elliptic orbit, we shall fix the initial values by assuming an elliptic orbit given by

$$\mathsf{r} = \frac{a(1-e^2)}{1+e\cos f},$$

where a is a semimajor axis, e is the eccentricity, and f is true anomaly. Since the orbital plane is not, in general, $\mathsf{z} = 0$, we have to introduce three angular variables: the argument of periapsis ω, the ascending node Ω, and the inclination angle I.

We have the relations between the position $\mathsf{r} = (\mathsf{x}, \mathsf{y}, \mathsf{z})$ of the component of a binary and the orbital parameters $(\omega, \Omega, a, e, I, f)$ as

$$\begin{pmatrix}\mathsf{x}\\ \mathsf{y}\\ \mathsf{z}\end{pmatrix} = \mathsf{r}\begin{pmatrix}\cos\Omega\cos(\omega+f) - \sin\Omega\sin(\omega+f)\cos I\\ \sin\Omega\cos(\omega+f) + \cos\Omega\sin(\omega+f)\cos I\\ \sin(\omega+f)\sin I\end{pmatrix}. \tag{5.9}$$

The initial position of a binary can be fixed by the orbital parameters. As for the initial velocity, we have the relation between the mean anomaly $\mathfrak{l}$ and the true anomaly f as

$$d\mathfrak{l} = (1-e^2)^{\frac{3}{2}}(1+e\cos f)^{-2}df. \tag{5.10}$$

In Newtonian dynamics, $\mathfrak{l} = n(\tau-\tau_0)$, where n is the mean motion. Hence, in this approximation, the time derivative $(d/d\tau)$ is given by the derivative with respect to the true anomaly (d/df).

Assuming $f=0$ at $\tau=0$, we find

$$\tilde{\mathsf{x}}(0) = (1-e_0)[\cos\Omega_0\cos\omega_0 - \sin\Omega_0\sin\omega_0\cos I_0],$$
$$\tilde{\mathsf{y}}(0) = (1-e_0)[\sin\Omega_0\cos\omega_0 + \cos\Omega_0\sin\omega_0\cos I_0],$$
$$\tilde{\mathsf{z}}(0) = (1-e_0)\sin\omega_0\sin I_0,$$

and

$$\frac{d\tilde{\mathsf{x}}}{d\tilde{\tau}}(0) = -\sqrt{\frac{1+e_0}{1-e_0}}[\cos\Omega_0\sin\omega_0 + \sin\Omega_0\cos\omega_0\cos I_0],$$
$$\frac{d\tilde{\mathsf{y}}}{d\tilde{\tau}}(0) = \sqrt{\frac{1+e_0}{1-e_0}}[-\sin\Omega_0\sin\omega_0 + \cos\Omega_0\cos\omega_0\cos I_0],$$
$$\frac{d\tilde{\mathsf{z}}}{d\tilde{\tau}}(0) = \sqrt{\frac{1+e_0}{1-e_0}}\cos\omega_0\sin I_0.$$

Hence, when we prepare the initial orbital parameters $(e_0,\ I_0,\ \omega_0,\ \Omega_0)$, we can provide the initial data for the normalized evolution equations (4.9)–(4.14).

C. Binary motion near ISCO radius

In a hierarchical triple system, there are several important features. One is the so-called von Zeipel-Lidov-Kozai (vZLK) oscillations. If the system is inclined more than some critical angle, there appears an oscillation between the eccentricity and inclination angle. The second interesting feature is an orbital flip, which may appear when the inclination angle evolves into near 90°. The last one which we show is a chaotic feature in the long-time evolution.

Here, we show our numerical results. In order to discuss the properties of a binary orbit, it is more convenient to use the orbital parameters assuming that the binary motion is close to an elliptic orbit.

In order to extract the orbital parameters from the orbit given by the Cartesian coordinates, one can use the osculating orbit when the orbit is close to an ellipse. However, one must be careful with the definitions of orbital elements when using the osculating method. For instance, the magnitude of the normalized Laplace-Runge-Lenz vector, which is defined by

$$\boldsymbol{e} \equiv \tilde{\mathbf{p}}\times(\tilde{\mathbf{r}}\times\tilde{\mathbf{p}}) - \frac{\tilde{\mathbf{r}}}{\tilde{\mathsf{r}}}, \tag{5.11}$$

is commonly used for a measure of orbital eccentricity, but it is not always appropriate. It may show an "apparent" rise in eccentricity or unphysical rapid oscillations especially when the eccentricity is very small [64]. We take caution and extract the elements' information from physical orbit. In that case, it may be better to define the eccentricity by the averaged one over one cycle as

$$\langle e\rangle \equiv \frac{\mathsf{r}_{\max}-\mathsf{r}_{\min}}{\mathsf{r}_{\max}+\mathsf{r}_{\min}},$$

where $\mathsf{r}_{\max}$ and $\mathsf{r}_{\min}$ correspond to orbital separation at adjacent turning points of an eccentric orbit.

The inclination angle I is defined as mutual inclination between angular momenta of the inner and outer binary. In the present case, since the outer binary is just a circular motion on the equatorial plane, the inclination is given by

$$I = \cos^{-1}\left(\frac{L_{\mathsf{z}}}{|\boldsymbol{L}|}\right),$$

where $\boldsymbol{L}\equiv\mathbf{r}\times\mathbf{p}$ is the angular momentum of a binary.

The other two essential angles Ω and ω governing the orientation of the orbital plane and the orbit are also computed in the postprocess. The line that marks the intersection of the orbital plane with the reference plane (the equatorial plane in the present case) is called the node line, and the point on the node line where the orbit passes above the reference plane from below is called the ascending node. The angle between the reference axis (say x-axis) and node line vector $\boldsymbol{N}$ is the longitude of ascending node Ω. First, node line is defined as

$$\boldsymbol{N} = \boldsymbol{e}_{\mathsf{z}}\times\boldsymbol{h},$$

where $\boldsymbol{e}_{\mathsf{z}}$ is normal to the reference plane (the unit vector in the z direction) and $\boldsymbol{h}=\boldsymbol{L}/\mu$ is specific angular momentum vector of a binary. Thus, Ω is computed as

$$\Omega = \cos^{-1}(N_{\mathsf{x}}/N).$$

The argument of periapsis ω is the angle between node line and periapsis measured in the direction of motion. Therefore,

$$\omega = \cos^{-1}\left(\frac{\boldsymbol{N}\cdot\boldsymbol{e}}{Ne}\right).$$

When the orbit can be approximated well by the osculating one, $\boldsymbol{e}$ is given by the normalized Laplace-Runge-Lenz vector (5.11). Otherwise, we define the averaged eccentricity vector by

$$\langle\boldsymbol{e}\rangle \equiv -\frac{(\mathbf{r}_{\min}+\mathbf{r}_{\max})}{(\mathsf{r}_{\min}+\mathsf{r}_{\max})}$$

pointing towards the periapsis, where $\mathbf{r}_{\max}$ and $\mathbf{r}_{\min}$ are numerical data of position vector. We have used both definitions and found that most results agree well.

1. Firmness of a binary and stability

As we discuss in Sec. V A, a binary near SMBH may be broken when the tidal force by SMBH is stronger than the mutual gravitational attractive force of a binary. We introduce a firmness parameter of a binary $\mathfrak{f}$ defined by

$$\mathfrak{f} \equiv \frac{\text{gravitational force}}{\text{tidal force by SMBH}} = \frac{Gm_1m_2/\ell_{\text{binary}}^2}{\mu \mathfrak{r}_g \ell_{\text{binary}}/\mathfrak{r}_0^3} = \left(\frac{m_1+m_2}{2M}\right)\left(\frac{\mathfrak{r}_0}{\ell_{\text{binary}}}\right)^3 \approx \frac{1}{\epsilon^2}\left(\frac{\mathfrak{r}_0}{\mathfrak{r}_g}\right).$$

If the firmness parameter $\mathfrak{f}$ is smaller than $O(1)$, we expect that the tidal force will break a binary. Hence, $\mathfrak{f} > 1$ is a necessary condition for stability of a binary. The condition against chaotic instability is

$$\mathfrak{f} \gtrsim \frac{C_{\text{chaotic}}^3}{2}\left(\frac{M}{m_1+m_2}\right)^{(3p-1)} \equiv \mathfrak{f}_{\text{chaotic}}.$$

We find $\mathfrak{f}_{\text{chaotic}} \sim 240$ for the criterion 1 with $m_1 = m_2 = 10M_\odot, M = 10^8 M_\odot$, or $\mathfrak{f}_{\text{chaotic}} \sim 69f$ for the criterion 2. Hence we may expect a chaotic feature for $1 < \mathfrak{f} \lesssim \mathfrak{f}_{\text{chaotic}}$.

When we are interested in a binary motion near SMBH, the tidal stability condition gives $\epsilon \le O(1)$, while the chaotic stability condition becomes $\epsilon \le$ a few tenths. We can confirm numerically that our present system is really unstable when $\epsilon \ge 0.5$. In what follows, we numerically analyze a binary system under the conditions of $\epsilon \le 0.4$.

2. von Zeipel-Lidov-Kozai oscillation

Here, we show some numerical examples, which show the vZLK oscillations in the long-time evolution.

We expect the vZLK oscillations to occur when the inclination angle is larger than the critical value. Under the quadrupole approximation in a Newtonian hierarchical system, the critical inclination angle is given by $I_{\text{crit}}^{(\text{N})} = \sin^{-1}\sqrt{2/5} \approx 39.23°$. In the present model, it can be obtained by the double-averaging analysis of the Lagrange planetary equations, which shows that the critical value is slightly larger as the radius $\mathfrak{r}_0$ gets smaller, and it increases to 41.6° near the ISCO radius (see Appendix B 2). It seems hard to obtain the exact critical value by numerical simulations, although we have found consistent results.

The typical timescale of the vZLK oscillations is given by [24,45,65]

$$T_{\text{vZLK}} \sim \frac{P_{\text{out}}^2}{P_{\text{in}}}, \tag{5.12}$$

where P_{in} and P_{out} are the periods of an inner binary and of an outer binary, respectively. For a hierarchical triple system, since $P_{\text{in}} \ll P_{\text{out}}$, $T_{\text{vZLK}} \gg P_{\text{out}}$, which means that the vZLK oscillation is a secular effect.

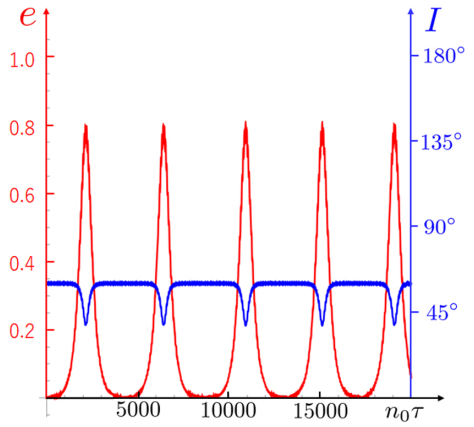

FIG. 2. This figure shows vZLK oscillation between orbital eccentricity e (the red curve) and relative inclination I (the blue curve). For this particular model (model Ic), we choose $\mathfrak{r}_0 = 3.5\mathfrak{r}_g$ and $\epsilon = 0.1$. The initial data is $e_0 = 0.01$, $I_0 = 60°$, $\omega_0 = 60°$, and $\Omega_0 = 30°$.

In the first model (model Ic), we choose $\mathfrak{r}_0 = 3.5\mathfrak{r}_g$ and $\epsilon = 0.1$. It corresponds to $a_0 = 0.0023\mathfrak{r}_g \approx 0.0045$ AU for $m_1 = m_2 = 10M_\odot$ and $M = 10^8 M_\odot$. Since $G(m_1+m_2)/c^2 \approx 30$ km $\ll a_0$, the binary motion can be described by a Newtonian orbit in a local inertial frame. We then adopt the initial conditions as the eccentricity $e_0 = 0.01$ and inclination $I_0 = 60°$. The numerical results are given in Figs. 2 and 3.

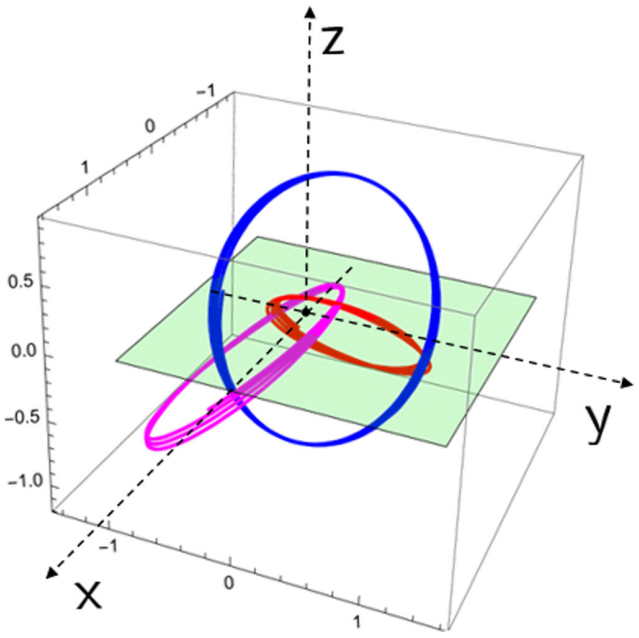

FIG. 3. Typical orbits in the same model as Fig. 2. The red, blue, and magenta curves denote a few cycles near $n_0\tau = 2120$, 4150, and 6385 respectively. The inclination angles of red, blue, and magenta curves are $I \approx 38.5°$, 61.1°, and 38.3°, while the eccentricities of those curves are $e \approx 0.80$, 0.0017, and 0.80, respectively.

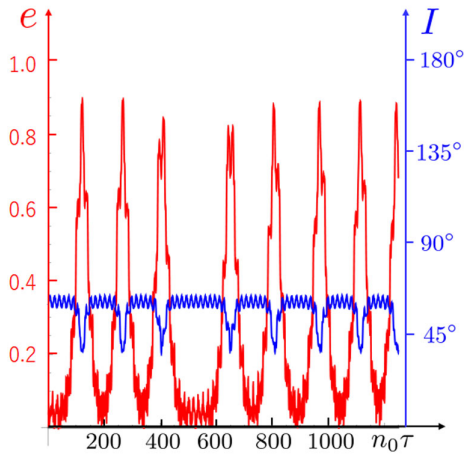

FIG. 4. Chaotic vZLK oscillation. The red and blue curves denote the eccentricity and the inclination. For this model (model IIc), we choose $\mathfrak{r}_0 = 3.5\mathfrak{r}_g$ and $\epsilon = 0.4$. The initial data is $e_0 = 0.01$, $I_0 = 60°$, $\omega_0 = 60°$, and $\Omega_0 = 30°$.

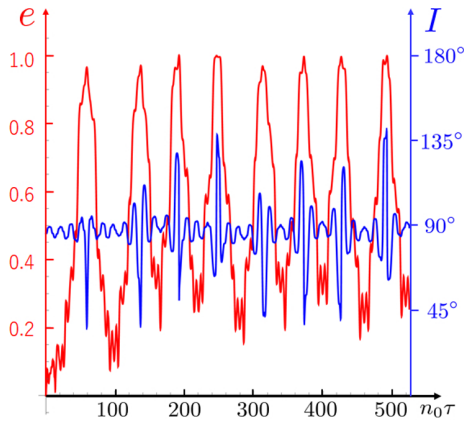

FIG. 5. Orbital flip in vZLK oscillation (model IIa). We choose $\mathfrak{r}_0 = 3.5\mathfrak{r}_g$ and $\epsilon = 0.4$. The initial data is $e_0 = 0.01$, $I_0 = 85°$, $\omega_0 = 60°$, and $\Omega_0 = 30°$. The red and blue curves denote the eccentricity and the inclination. The inclination angle evolves beyond 90° several times.

The vZLK oscillation period is obtained numerically as $n_0 T_{\rm vZLK} \sim 4000$. Since $n_0 P_{\rm in} \sim 2\pi$ and $\omega_0 P_{\rm out} \sim 2\pi$, we can evaluate it by Eq. (5.12) as $n_0 P_{\rm out}^2/P_{\rm in} \sim 2\pi(n_0/\omega_0)^2 \sim 2500$, which is consistent with the above numerical value.

3. Chaotic feature

One of the well-known features of three body system is a chaotic behavior in a binary motion. The model given in the previous subsection shows a stable vZLK oscillation. The vZLK oscillation period is regular. The chaotic feature is not seen. This is just because a binary is extremely compact and very hard. The firmness parameter is $\mathfrak{f} \sim 350$.

However, if a binary is not so highly compact, we find some chaotic features. In Fig. 4, we show one example (model IIc). The model parameters are given by $\epsilon = 0.4$ and $\mathfrak{r}_0 = 3.5\mathfrak{r}_g$, and the initial parameters are chosen as $e_0 = 0.01$, $I_0 = 60°$, $\omega_0 = 60°$, and $\Omega_0 = 30°$. The larger value of ϵ corresponds to a larger-scale binary, i.e., the initial semimajor axis is $a_0 = 0.0058\mathfrak{r}_g \approx 0.0115$ AU. We can see clearly the vZLK oscillation, but the period is not strictly regular. Since the firmness parameter is $\mathfrak{f} \sim 22 > O(1)$, the system is still stable, but shows some irregular behaviors in the vZLK oscillations. The maximum values of the eccentricity is also random as shown in Fig. 4.

4. Orbital flip

Another interesting feature is an orbital flip, i.e., an inclination angle goes beyond 90°. It may occur when the initial inclination angle is near 90°.

In Fig. 5, we find that the orbital flip accompanying vZLK oscillations occurs periodically. The model parameters are given by $\epsilon = 0.4$ and $\mathfrak{r}_0 = 3.5\mathfrak{r}_g$, and the initial parameters are chosen as $e_0 = 0.01$, $I_0 = 85°$, $\omega_0 = 60°$, and $\Omega_0 = 30°$ (model IIa). The inclination blue curve in Fig. 5 evolves beyond 90° several times, but the time period is irregular.

One interesting observation is there exists a strong correlation between an orbital flip and large eccentricity. When an orbital flip occurs, the eccentricity becomes very close to unity.

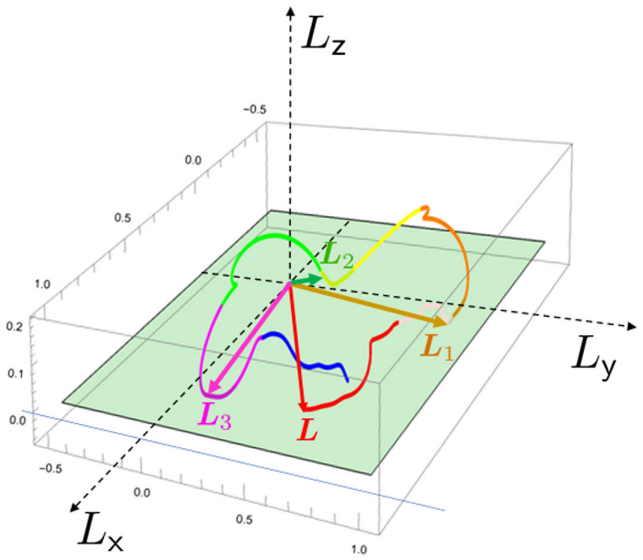

FIG. 6. Time evolution of angular momentum. The parameters and initial conditions are the same as those in Fig. 5. The red, light red, orange, yellow, green, magenta, and blue curves denote the angular momentum vectors in the periods $n_0\tau = 40$–50, $50-60, 60-70, 70-80, 80-90, 90-100$, and 100–110, respectively. The z-components of $\boldsymbol{L}_1$, $\boldsymbol{L}_2$, and $\boldsymbol{L}_3$ become negative.

In Fig. 6, we show the time evolution of the angular momentum vector, which is defined by $\boldsymbol{L} = \mathbf{r} \times \mathbf{p}$. The z-component of the angular momentum becomes negative near $n_0\tau \approx 60$–$62, 73 - 80$, and 92–97. The corresponding vectors are shown by the colored arrows $\boldsymbol{L}_1$, $\boldsymbol{L}_2$, and $\boldsymbol{L}_3$, respectively.

5. Summary of various models

We summarize our numerical results in Table I. We have simulated three types of models (I, II, and III). The parameters of model I, model II, and model III are ($\mathfrak{r}_0 = 3.5\mathfrak{r}_g$, $\epsilon = 0.1$), ($\mathfrak{r}_0 = 3.5\mathfrak{r}_g$, $\epsilon = 0.4$), and ($\mathfrak{r}_0 = 7\mathfrak{r}_g$, $\epsilon = 0.1$), respectively. For each model, we choose the initial data as (a) $e_0 = 0.01, I_0 = 85°$, (b) $e_0 = 0.9, I_0 = 85°$, (c) $e_0 = 0.01, I_0 = 60°$, and (d) $e_0 = 0.9, I_0 = 60°$. The initial argument of periapsis and ascending node are chosen as $\omega_0 = 60°$ and $\Omega_0 = 30°$ for all models. We also performed the simulation with different values of those two parameters; the results do not vary much.

In model I, since the binary is very compact (the firmness parameter $\mathfrak{f} \sim 350 > \mathfrak{f}_{\rm chaotic}$), it is very stable. As shown in Fig. 2, we find the regular vZLK oscillation, although the oscillation period $T_{\rm vZLK}$ is not strictly constant but slightly disperse within 1–9%. When the initial eccentricity is large (model Ib and Id), the oscillation period gets smaller and minimum eccentricity becomes larger. Except for model Ic, the vZLK oscillation type is the so-called libration, which shows the oscillation of the argument of periapsis around 90°. In model Ic, the vZLK oscillation seems to be the rotation type, which denotes the argument of periapsis increases monotonically. However in the present model, it does increase on average but not monotonically (sometimes going back and forth).

For model II, the binary is slightly less compact (the firmness parameter $\mathfrak{f} \sim 22 < \mathfrak{f}_{\rm chaotic}$). It is still stable but becomes irregular both in the oscillation period and in the amplitude as shown in Fig. 4. There appears to be dispersion in the maximum and minimum values of the eccentricity and inclination, whose values are shown in the bracket (). When the initial inclination angle is large (models IIa and IIb), we find irregular orbital flips. The vZLK oscillation is either libration type (models IIb and IId), in which the maximum and minimum angles of the argument of the periapsis disperse as shown by the brackets (), or irregular rotation type (models IIa and IIc), in which the inclination angle increases on average but not monotonically (sometimes going back and forth).

Model III is the case with a hard binary as model I, but its location is a little far from SMBH ($\mathfrak{r}_0 = 7\mathfrak{r}_g$). Hence the relativistic effect as well as the tidal force are smaller than those in model I. As a result, the vZLK oscillation becomes more regular and stable. The vZLK oscillation timescale is larger than that in model I because the outer orbital period $P_{\rm out}$ is larger.

D. Motion of the CM of a binary

Next we show the motion of the CM of a binary. In order to know how much the motion deviates from a circular motion with the radius $\mathfrak{r}_0$, we solve the radial perturbation equation (4.21). Using the previous numerical solutions, we integrate Eq. (4.21) with the initial conditions such that $\mathfrak{r}_{(1)}(0) = 0$ and $\dot{\mathfrak{r}}_{(1)}(0) = 0$. Here, we discuss some typical cases.

1. Model Ia

In this case, we find stable and regular oscillations with the period $T_{\rm osc} \equiv 2\pi/k \approx 2.65 P_{\rm out}$, where k is defined by Eq. (4.22) and $P_{\rm out} = 2\pi/\mathfrak{w}_0$ is the period of the circular motion. The oscillation center is given by $\langle \mathfrak{r}_1 \rangle \approx 1.60 \times 10^{-4}\mathfrak{r}_0$ with the amplitude $\Delta\mathfrak{r}_1 \approx 1.71 \times 10^{-4}\mathfrak{r}_0$, but the center increases to $2.18 \times 10^{-4}\mathfrak{r}_0$ when the eccentricity becomes close to unity, keeping the oscillation amplitude $\Delta\mathfrak{r}_1$ to be constant [see Fig. 7 (left)].

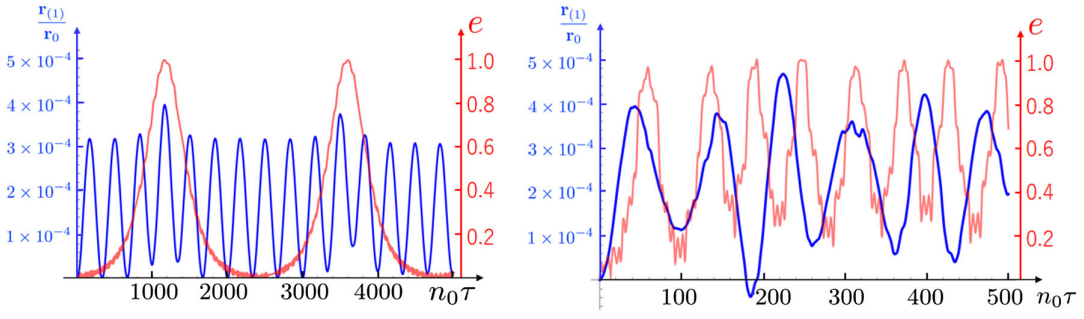

FIG. 7. The radial deviation $\mathfrak{r}_{(1)}$ normalized by the radius of the circular orbit $\mathfrak{r}_0$ are shown by blue curves for model Ia (left) and model IIa (right). The deviation from a circular orbit in model Ia is regular oscillation around $\langle \mathfrak{r}_1 \rangle$, which is the mean of $\mathfrak{r}_{(1)}$. Note that $\langle \mathfrak{r}_1 \rangle$ increases when the eccentricity increases (red curve). While in model IIa, it results in irregular oscillations without correlation with the eccentricity (the red curve).

TABLE I. The properties of the vZLK oscillations. The oscillations in models I and III are regular, although there are small amounts of dispersion in the vZLK oscillation timescale. For model II, the oscillations are irregular and there appears to be dispersion in the maximum and minimum values of the eccentricity and inclination, whose values are shown in the bracket (). $\mathbb{L}$ and $\mathbb{R}$ denote libration and rotation types, respectively. $\mathbb{R}^*$ means that the argument of periapsis does increase on average but not monotonically, and sometimes going back and forth.

Model	$\mathfrak{r}_0$	ϵ	a_0	e_0	I_0	ω_0	Ω_0	vZLK oscillation type	$n_0 T_{\rm vZLK}$	$e_{\rm min}/e_{\rm max}$	$I_{\rm min}/I_{\rm max}$	Orbital flip
Ia				0.01	85°	60°	30°	$\mathbb{L}\,[36° \le \omega \le 144°]$	2396–2430	0.01/0.995	39.1°/85.5°	No
Ib				0.9	85°	60°	30°	$\mathbb{L}\,[55° \le \omega \le 125°]$	580–600	0.672/0.998	54.8°/87.5°	No
Ic	$3.5\mathfrak{r}_g$	0.1	$0.0046\mathfrak{r}_g$	0.01	60°	60°	30°	$\mathbb{R}^*$	3600–4300	0.003/0.8	38.5°/60.5°	No
Id				0.9	60°	60°	30°	$\mathbb{L}\,[56° \le \omega \le 124°]$	753–770	0.49/0.95	47.3°/74.3°	No
IIa				0.01	85°	60°	30°	$\mathbb{R}^*$	50–78	$(0.15-0.34)/(0.97-1.00)$	$(33.6°-42.0°)/(137.9°-143.9°)$	Yes (irregular)
IIb				0.9	85°	60°	30°	$\mathbb{L}\,[(50°-53°) \le \omega \le (126°-131°)]$	39–44	$(0.533-0.589)/(0.978-0.999)$	$(50.2°-53.7°)/(126.4°-128.6°)$	Yes (irregular)
IIc	$3.5\mathfrak{r}_g$	0.4	$0.0116\mathfrak{r}_g$	0.01	60°	60°	30°	$\mathbb{R}^*$	116–250	$(0.04-0.08)/(0.82-0.90)$	$(36.5°-37.7°)/(59°-65°)$	No
IId				0.9	60°	60°	30°	$\mathbb{L}\,[(50°-56°) \le \omega \le (124°-130°)]$	54–60	$(0.41-0.49)/(0.92-0.97)$	$(43°-46°)/(69°-75°)$	No
IIIa				0.01	85°	60°	30°	$\mathbb{L}\,[38° \le \omega \le 142°]$	6776–6928	0.009/0.997	39.1°/85.2°	No
IIIb				0.9	85°	60°	30°	$\mathbb{L}\,[56° \le \omega \le 124°]$	1585–1628	0.675/0.998	55.1°/87.2°	No
IIIc	$7\mathfrak{r}_g$	0.1	$0.0073\mathfrak{r}_g$	0.01	60°	60°	30°	$\mathbb{L}\,[44° \le \omega \le 136°]$	9450–10600	0.004/0.792	38.3°/60.3°	No
IIId				0.9	60°	60°	30°	$\mathbb{L}\,[56° \le \omega \le 124°]$	2045–2074	0.493/0.949	47.5/74.5	No

There exists a good correlation between the shift of the oscillation center and the eccentricity. Since the oscillation amplitude is very small compared with the circular radius $\mathfrak{r}_0$, the deviations from the circular motion can be treated as perturbations, which confirms our approach.

2. Model IIa

In this case, the vZLK oscillation is stable but irregular. As a result, we find irregular oscillations of the CM as shown by a blue curve in Fig 7 (right). There is no correlation with the eccentricity e. Although the oscillations are irregular, the amplitude is very small and therefore the deviation from the circular motion can be treated as stable perturbations.

3. Other models

We summarize the results in Table II for the models given in Table I. We find that models I and III give stable and regular oscillations of the CM. It is just because those binary motions also show stable and regular vZLK oscillations. On the other hand, model II shows irregular oscillations because of the irregular vZLK oscillations in those binary motions.

TABLE II. The oscillations of the CM, which are the radial deviations from a circular geodesic motion. $\langle \mathfrak{r}_1 \rangle$ denotes the center of the oscillations, while $\Delta\mathfrak{r}_1$ gives the amplitude of the oscillations (or dispersion for the irregular oscillations [model II]). The typical oscillation period is given by $T_{\rm osc} \equiv 2\pi/k$, where k is defined by Eq. (4.22).

Model	$\mathfrak{r}_0$ (AU)	a_0 (AU)	ϵ	$\mathfrak{f}$	e_0	I_0	$[\langle \mathfrak{r}_1 \rangle \pm \Delta\mathfrak{r}_1]/\mathfrak{r}_0$	$T_{\rm ocs}/P_{\rm out}$	Oscillation property
Ia					0.01	85°	$[(1.60-2.18) \pm 1.71] \times 10^{-4}$		Regular (good correlation with e)
Ib					0.9	85°	$[0.18 \pm 3.51] \times 10^{-3}$		Regular
Ic	6.91	0.0091	0.1	350	0.01	60°	$[(7.01-7.37) \pm 7.04] \times 10^{-4}$	2.65	Regular (good correlation with e)
Id					0.9	60°	$[(4.09-4.40) \pm 4.51] \times 10^{-4}$		Regular (good correlation with e)
IIa					0.01	85°	$[(1.60-2.91) \pm 1.88] \times 10^{-4}$		Irregular (no correlation with e)
IIb					0.9	85°	$[(2.89-3.18) \pm 2.85] \times 10^{-4}$		Regular (no correlation with e)
IIc	6.91	0.0229	0.4	21.9	0.01	60°	$[(4.30-5.77) \pm 6.09] \times 10^{-4}$	2.65	Irregular (no correlation with e)
IId					0.9	60°	$[(4.05-4.31) \pm 4.41] \times 10^{-4}$		Irregular (no correlation with e)
IIIa					0.01	85°	$[(1.23-1.56) \pm 1.28] \times 10^{-5}$		Regular (good correlation with e)
IIIb					0.9	85°	$[(1.22-1.43) \pm 1.35] \times 10^{-5}$		Regular (good correlation with e)
IIIc	13.8	0.0144	0.1	700	0.01	60°	$[(5.78-5.98) \pm 5.83] \times 10^{-5}$	1.32	Regular (good correlation with e)
IIId					0.9	60°	$[(3.14-3.33) \pm 3.38] \times 10^{-5}$		Regular (good correlation with e)

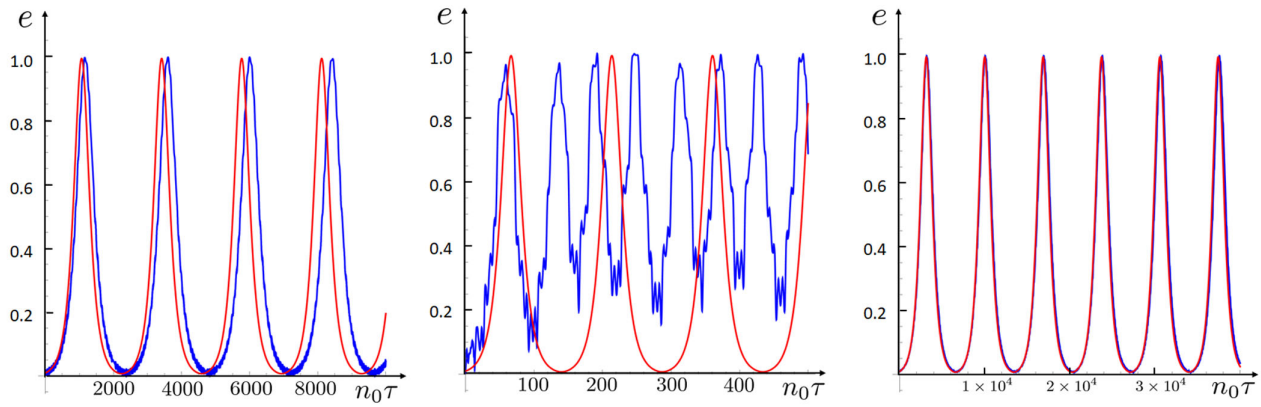

FIG. 8. The evolution of the eccentricity for models Ia (left), IIa (center), and IIIa (right). The red curves denote the results by the double-averaging (DA) approach, while the blue ones by the direct integration (DI) method. For models Ia and IIIa, the two results agree well, but for model IIa, they do not agree well.

E. Comparison with double-averaging approach

In Appendix B, we present one of the standard approaches on a hierarchical triple system, which involves the Lagrange planetary equations for the orbital parameters. Since we are interested in the long-time behavior such as the vZLK mechanism, taking averages of the Hamiltonian over two periods of the inner and outer binaries, we can analyze the simplified doubly-averaged planetary equations.

Here, we compare our numerical results with those obtained in the double-averaging (DA) approach. We show the evolution of the eccentricity for models Ia, IIa and IIIa in the left, center, and right panels of Fig. 8, respectively.

For model Ia, two results agree very well although the oscillation period of the DA approach is slightly longer than that of the direct integration (DI) method. For model IIa, the DA approach gives regular periodic oscillations, but the DI method shows irregular chaotic oscillations. The two results do not agree well, although the maximum values of the eccentricity are almost the same. For model IIIa, two results agree almost completely. For other models, we also find the similar results.

We conclude that the DA approach for models I and III may give good results although the period of oscillations deviates slightly. On the other hand, for model II, which shows chaotic features in the vZLK oscillations, the DA approach does not give correct results.

VI. CONCLUDING REMARKS

In this paper, we discuss the motion of a binary system near SMBH. Using Fermi-normal coordinates, we set up a Newtonian self-gravitating system in the local proper reference frame. Assuming a circular geodesic observer around a Schwarzschild SMBH, we write down the equations of motion of a binary. To remove the interaction terms between the CM of a binary and its relative coordinates, we introduce a small acceleration of the observer. As a result, the CM follows the observer's orbit, but its motion deviates from an exact geodesic. Since the relative motion is decoupled from the system, we first solve it, and then find the motion of the CM by the perturbation equations with the small acceleration, which is given by the relative motion.

We show that there appear to be vZLK oscillations when a binary is compact enough and the inclination angle is larger than the critical value. If the firmness parameter $\mathfrak{f}$ is larger than a few hundred, the oscillations are regular. However when $\mathfrak{f}$ is around a few tens, although we find the stable vZLK oscillations, the oscillations become irregular both in the oscillation period and in the amplitude. Especially if the initial inclination is large, we find an orbital flip.

One of the most interesting and important subjects of a binary system near SMBH is the gravitational waves. When the vZLK oscillations are found in a binary motion, we expect a large amount of GW emissions because the eccentricity becomes large. The large eccentricity also provides much higher frequencies than that from a circular binary [25,27,42]. Another interesting point on the GWs from the vZLK oscillations is that the large amount of the GW emissions repeats periodically with the vZLK oscillation timescale. It is a good advantage in the observations because we have a certain preparation time for next observations.

There are two GW sources in a hierarchical triple system: One GW source is from an inner binary and the other is from the outer binary. The timescale of the emission of gravitational waves from a circular binary is evaluated as [66]

$$\tau_{\rm GW} = \frac{5}{256}\frac{c^5 R_0^4}{G^3 m^2 \mu},$$

where $m = m_1 + m_2$ and $\mu = m_1 m_2/(m_1 + m_2)$ and R_0 is the initial distance. Hence, the ratio of the timescale of an outer binary to that of an inner binary is

$$\frac{\tau_{\rm outer}}{\tau_{\rm inner}} = \frac{m_1 m_2}{M^2}\left(\frac{\mathfrak{r}_0}{\ell_{\rm binary}}\right)^4.$$

In the present model, as we discuss in Sec. V A, we have some constraints. From the stability condition of a binary (5.1), we have

$$\frac{\ell_{\rm binary}}{\mathfrak{r}_0} \lesssim \left(\frac{m_1+m_2}{2M}\right)^{1/3},$$

while from the validity of Newtonian dynamics, we find

$$\frac{\ell_{\rm binary}}{\mathfrak{r}_0} \gtrsim \left(\frac{m_1+m_2}{2M}\right)\frac{\mathfrak{r}_g}{\mathfrak{r}_0}.$$

If a binary exists near the ISCO radius ($\mathfrak{r}_0 \sim 3\mathfrak{r}_g$), we find

$$2\times 10^{-5} \lesssim \frac{\tau_{\rm outer}}{\tau_{\rm inner}} \lesssim 8\times 10^{16}.$$

Hence, in most cases, gravitational waves from the outer orbit are less effective compared with those from the inner binary. However when the binary is close to instability range, it is not the case. In fact, in our examples discussed in this paper, if we assume a circular binary, we find

$$\frac{\tau_{\rm outer}}{\tau_{\rm inner}} \sim \begin{cases} 3\times 10^{-3} & \text{(model I)} \\ 8\times 10^{-5} & \text{(model II)} \\ 8\times 10^{-3} & \text{(model III)} \end{cases}$$

The GWs from the outer binary become much larger than those from the inner binary. However if there exists the vZLK oscillation, the emission timescale is reduced by the factor [67]

$$F(e_{\rm in}) \approx \frac{768}{429}(1-e_{\rm in}^2)^{7/2},$$

when $e_{\rm in} \approx 1$. As a result, the GWs from the inner binary may become larger that those from the outer binary.

In recent years, three-body systems and the emission of GWs from them have received significant attention [25–27,36–43]. Our future work will involve evaluating the GWs from the present hierarchical triple setting using the black hole perturbation approach, since near the ISCO radius the quadrupole formula may not be valid [68].

In this paper, we assume that the CM of a binary moves along a circular orbit, but an eccentric orbit is interesting to be studied since the vZLK oscillation may be modulated on a longer timescale [69–73]. However, for such a highly eccentric orbit, the present proper reference frame expanded up to the second order of the spatial coordinates $x^{\hat{a}}$ may not be sufficient. We may need higher-order terms in the metric, where the derivatives of the Riemann curvature appear [51,52]. Although the basic equations are very complicated, such an extension is straightforward.

Another natural direction would be an extension to a rotating SMBH that may allow us to study the precession of the binary orbit around the Kerr black hole. Such systems can reveal the impact of spin on GWs emitted from a nearby binary. Recent research [59] considers the secular dynamics of the binary system distorted by a much larger Kerr black hole's tidal forces. This is done by deriving the magnetic and electric tidal moment at quadrupole orders.

ACKNOWLEDGMENTS

We thank Luc Blanchet, Vitor Cardoso, Eric Gourgoulhon, and Haruka Suzuki for useful discussions. This work was supported in part by JSPS KAKENHI Grants No. JP17H06359, JP19K03857 (K. M.), and by JP20K03953, JP23K03222 (H. O.). P. G. acknowledges support from C. V. Raman fellowship grant. K. M. would like to acknowledge the Yukawa Institute for Theoretical Physics at Kyoto University, where the present work was begun during the Visitors Program of FY2022. He would also like to thank Niels Bohr Institute/Niels Bohr International Academy, the Max Planck Institute for Gravitational Physics (Albert Einstein Institute), the laboratory AstroParticle and Cosmology (APC), and Center for astrophysics and gravitation (CENTRA)/Instituto Superior Técnico, where most of this work was performed.

APPENDIX A: COPLANAR BINARY

In this Appendix, we analyze the motion of a coplanar binary, that is $\mathsf{z}=0, \mathsf{p}_z=0$. It is an exact solution for Eqs. (4.11) and (4.14).

1. Coplanar motion: Numerical results

In the case of coplanar motion of a binary, the relative inclination angle I is always zero. We then have the coupled equations (4.9), (4.10), (4.12), and (4.13) for x and y. We first show numerical results for models I ($\mathfrak{r}_0 = 3.5\mathfrak{r}_g, \epsilon = 0.1$) and II ($\mathfrak{r}_0 = 3.5\mathfrak{r}_g, \epsilon = 0.4$) in Fig. 9. We choose the initial conditions as $e_0 = 0.9$ and $\omega_0 = 60°$. For model I, as shown in Fig. 9 (left), the orbit is approximately elliptic, but the periapsis is rotating because of relativistic effect and the shift is quite regular. On the other hand, for model II, we find some irregular behaviors in the orbit as shown in Fig. 9 (right). As discussed in the text, this model is not tightly bounded (the firmness parameter $\mathfrak{f} \sim 22 < \mathfrak{f}_{\rm chaotic}$) and the effects of the tidal force by SMBH is not so small. As a result, the system shows some chaotic features. In the present coplanar case, the orbital shape is deformed from an ellipse.

It is further confirmed by the time evolution of the eccentricity, which is given in Fig. 10. For model I, the eccentricity is almost constant ($e \sim 0.9$). On the other hand,

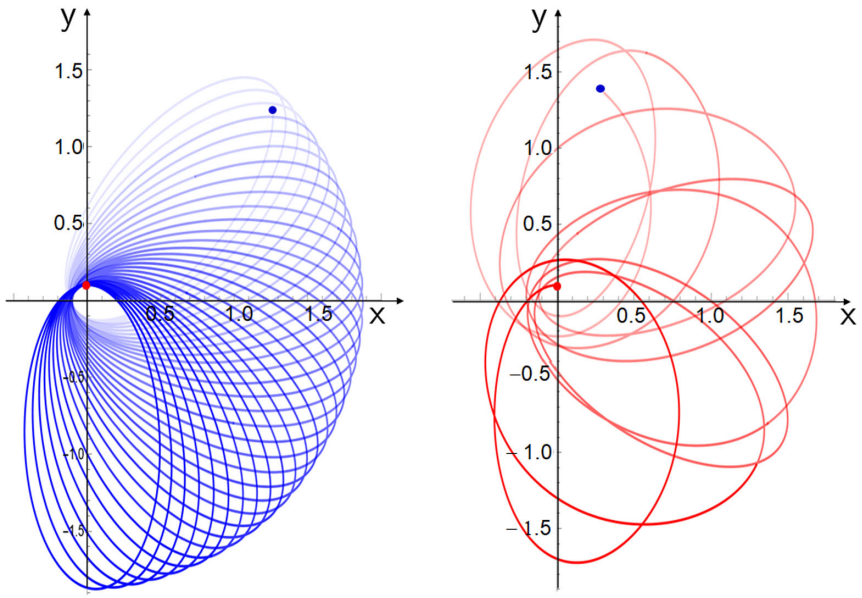

FIG. 9. The coplanar orbits for model I (left) and for model II (right). We choose the initial eccentricity $e_0 = 0.9$. The orbits start from the red point, and end at the blue point [($n_0\tau = 200$ (model I) and $n_0\tau = 50$ (model II)].

for model II, it oscillates irregularly between $e \sim 0.7$ and 0.9. Although the orbital shape is not well approximated by an ellipse, we evaluate the eccentricity by the osculating orbit. If we use the average eccentricity over one cycle, the eccentricity oscillates between $\langle e \rangle \sim 0.75$ and 0.87, which is slightly different from the values in Fig. 10.

2. Circular motion

There exists an exact circular motion of a binary as follows: Assuming a circular solution as

$$\zeta \equiv \mathsf{x} + i\mathsf{y} = \rho_0 \exp\left[i\theta(\tau)\right], \quad \text{with} \quad \theta(\tau) = \bar{\theta}(\tau) + \mathfrak{w}_{\rm ds}\tau,$$

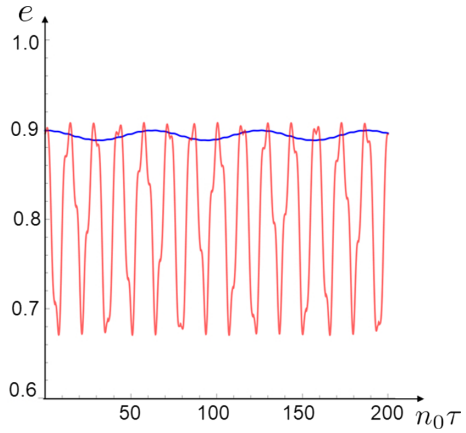

FIG. 10. Time evolution of the eccentricity for model I (the blue curve) and for model II (the red curve). The eccentricity for model I is almost constant ($e \approx 0.9$), while for model II it oscillates irregularly between $e \sim 0.7$ and 0.9.

where the radius ρ_0 is constant, we find two equations for $\bar{\theta}$ as

$$-\dot{\bar{\theta}}^2 + \frac{G(m_1+m_2)}{\rho_0^3} - \frac{\mathfrak{r}_g}{4\mathfrak{r}_0^3}(1+3\mathfrak{r}_0^2\mathfrak{w}_0^2) - \frac{3\mathfrak{r}_g}{4\mathfrak{r}_0^3}(1+\mathfrak{r}_0^2\mathfrak{w}_0^2)\cos(2(\bar{\theta}+2\mathfrak{w}_{\rm R}\tau)) = 0, \tag{A1}$$

$$\ddot{\bar{\theta}} + \frac{3\mathfrak{r}_g}{4\mathfrak{r}_0^3}(1+\mathfrak{r}_0^2\mathfrak{w}_0^2)\sin(2(\bar{\theta}+2\mathfrak{w}_{\rm R}\tau)) = 0. \tag{A2}$$

Since the derivative of Eq. (A1) with respect to τ gives Eq. (A1) unless $\bar{\theta} = 0$, we first solve Eq. (A2). Setting $\eta \equiv 2(\bar{\theta} + 2\mathfrak{w}_{\rm R}\tau)$, we find

$$\ddot{\eta} + \frac{3\mathfrak{r}_g}{2\mathfrak{r}_0^3}(1+\mathfrak{r}_0^2\mathfrak{w}_0^2)\sin\eta = 0,$$

which can be integrated as

$$\dot{\eta}^2 - \frac{3\mathfrak{r}_g}{\mathfrak{r}_0^3}(1+\mathfrak{r}_0^2\mathfrak{w}_0^2)\cos\eta = \text{constant}.$$

By use of this equation, we can eliminate the term with $\cos\eta$ in Eq. (A1), resulting in $\dot{\eta}$ and $\dot{\bar{\theta}}$ to be constant. It follows that $\cos\eta = \cos(2(\bar{\theta}+2\mathfrak{w}_R\tau))$ is constant. We then obtain a solution such that

$$\bar{\theta} + 2\mathfrak{w}_{\rm R}\tau = \frac{n}{2}\pi,$$

where n is an integer. Equation (A1) becomes

$$-4\mathfrak{w}_{\rm R}^2 = -\frac{G(m_1+m_2)}{\rho_0^3} + \frac{\mathfrak{r}_g}{4\mathfrak{r}_0^3}(1+3\mathfrak{r}_0^2\mathfrak{w}_0^2) + \frac{3\mathfrak{r}_g}{4\mathfrak{r}_0^3}(1+\mathfrak{r}_0^2\mathfrak{w}_0^2)(-1)^n.$$

Since $\mathfrak{w}_{\rm R} = \sqrt{\mathfrak{r}_g/2\mathfrak{r}_0^3}$, we obtain two analytic solutions as follows: When n is even,

$$\rho_0 = \rho_0^{(+)} \equiv \sqrt[3]{\frac{(m_1+m_2)}{2M(1+\mathfrak{r}_0^2\mathfrak{w}_0^2)}}\mathfrak{r}_0, \tag{A3}$$

$$\theta = \theta^{(+)} \equiv \bar{\theta}^{(+)} + \mathfrak{w}_{\rm dS}\tau = (\mathfrak{w}_{\rm dS} - 2\mathfrak{w}_{\rm R})\tau + m\pi \quad (m \in \mathbb{Z}), \tag{A4}$$

while when n is odd,

$$\rho_0 = \rho_0^{(-)} \equiv \sqrt[3]{\frac{(m_1+m_2)}{M(1+\mathfrak{r}_0^2\mathfrak{w}_0^2)}}\mathfrak{r}_0, \tag{A5}$$

$$\theta = \theta^{(-)} \equiv \bar{\theta}^{(-)} + \mathfrak{w}_{\rm dS}\tau = (\mathfrak{w}_{\rm dS} - 2\mathfrak{w}_{\rm R})\tau + \left(m+\frac{1}{2}\right)\pi \quad (m \in \mathbb{Z}). \tag{A6}$$

Using these solutions, we can find the analytic solution for the motion of the CM of a binary. The relative coordinates (x, y, z) of a binary in the rotating proper frame are given by

$$\begin{aligned} x &= \mathsf{x}\cos(\mathfrak{w}_{\rm R}\tau) - \mathsf{y}\sin(\mathfrak{w}_{\rm R}\tau) \\ &= \rho_0^{(\pm)}\cos[(\mathfrak{w}_{\rm dS} - \mathfrak{w}_{\rm R})\tau + \phi_0^{(\pm)}], \\ y &= \mathsf{x}\sin(\mathfrak{w}_{\rm R}\tau) + \mathsf{y}\cos(\mathfrak{w}_{\rm R}\tau) \\ &= \rho_0^{(\pm)}\sin[(\mathfrak{w}_{\rm dS} - \mathfrak{w}_{\rm R})\tau + \phi_0^{(\pm)}], \\ z &= \mathsf{z} = 0, \end{aligned}$$

where $\rho_0^{(\pm)}$ are given by the previous solutions, and $\phi_0^{(+)} = m\pi$ and $\phi_0^{(-)} = (m+\frac{1}{2})\pi$. We then find the perturbation equation for $\mathfrak{r}_{(1)}$ as

$$\frac{d^2\mathfrak{r}_{(1)}}{d\tau^2} + k^2\mathfrak{r}_{(1)} + C^{(\pm)}\cos^2[(\mathfrak{w}_{\rm dS} - \mathfrak{w}_{\rm R})\tau + \phi_0^{(+)}] = 0, \tag{A7}$$

where

$$C^{(\pm)} \equiv [A + (\mathfrak{w}_{\rm dS} - \mathfrak{w}_{\rm R})B]\left(\rho_0^{(+)}\right)^2.$$

Since two independent solutions of the homogeneous equation are $\sin k\tau$ and $\cos k\tau$, introducing two unknown functions $u(\tau)$ and $v(\tau)$, we set

$$\mathfrak{r}_{(1)} = u(\tau)\sin k\tau + v(\tau)\cos k\tau.$$

Inserting this into Eq. (A7), we find

$$\ddot{u}\sin k\tau + \ddot{v}\cos k\tau + 2k(\dot{u}\cos k\tau - \dot{v}\sin k\tau) + C^{(\pm)}\cos^2[(\mathfrak{w}_{\rm dS} - \mathfrak{w}_{\rm R})\tau + \phi_0^{(\pm)}] = 0.$$

We assume one constraint equation such that

$$\dot{u}\sin k\tau + \dot{v}\cos k\tau = 0, \tag{A8}$$

which yields

$$\ddot{u}\sin k\tau + \ddot{v}\cos k\tau + k(\dot{u}\cos k\tau - \dot{v}\sin k\tau) = 0.$$

We then find

$$k(\dot{u}\cos k\tau - \dot{v}\sin k\tau) + C^{(\pm)}\cos^2[(\mathfrak{w}_{\rm dS} - \mathfrak{w}_{\rm R})\tau + \phi_0^{(\pm)}] = 0. \tag{A9}$$

From Eqs. (A8) and (A9), we obtain

$$\begin{aligned} \dot{u} &= -\frac{C^{(\pm)}}{k}\cos k\tau\cos^2[(\mathfrak{w}_{\rm dS} - \mathfrak{w}_{\rm R})\tau + \phi_0^{(\pm)}], \\ \dot{v} &= \frac{C^{(\pm)}}{k}\sin k\tau\cos^2[(\mathfrak{w}_{\rm dS} - \mathfrak{w}_{\rm R})\tau + \phi_0^{(\pm)}]. \end{aligned}$$

We can integrate these equations as

$$\begin{aligned} u &= u_0 - \frac{C^{(\pm)}}{2k}\left[\frac{1}{k}\sin k\tau + \frac{1}{2}\left(\frac{\sin[(k+2(\mathfrak{w}_{\rm dS} - \mathfrak{w}_{\rm R}))\tau + 2\phi_0^{(\pm)}]}{k+2(\mathfrak{w}_{\rm dS} - \mathfrak{w}_{\rm R})} + \frac{\sin[(k-2(\mathfrak{w}_{\rm dS} - \mathfrak{w}_{\rm R}))\tau - 2\phi_0^{(\pm)}]}{k-2(\mathfrak{w}_{\rm dS} - \mathfrak{w}_{\rm R})}\right)\right], \\ v &= v_0 - \frac{C^{(\pm)}}{2k}\left[\frac{1}{k}\cos k\tau + \frac{1}{2}\left(\frac{\cos[(k+2(\mathfrak{w}_{\rm dS} - \mathfrak{w}_{\rm R}))\tau + 2\phi_0^{(\pm)}]}{k+2(\mathfrak{w}_{\rm dS} - \mathfrak{w}_{\rm R})} + \frac{\cos[(k-2(\mathfrak{w}_{\rm dS} - \mathfrak{w}_{\rm R}))\tau - 2\phi_0^{(\pm)}]}{k-2(\mathfrak{w}_{\rm dS} - \mathfrak{w}_{\rm R})}\right)\right], \end{aligned}$$

where u_0 and v_0 are integration constants. As a result, we obtain the general solution as

$$\mathfrak{r}_{(1)} = -\frac{C^{(\pm)}}{2k^2} + u_0\sin k\tau + v_0\cos k\tau - \frac{C^{(\pm)}}{2[k^2 - 4(\mathfrak{w}_{\rm dS} - \mathfrak{w}_{\rm R})^2]}\cos[2(\mathfrak{w}_{\rm dS} - \mathfrak{w}_{\rm R})\tau + 2\phi_0^{(\pm)}].$$

The initial conditions determine the integration constants u_0 and v_0. For example, if we assume $\mathfrak{r}_{(1)}(0)=0$ and $\dot{\mathfrak{r}}_{(1)}(0)=0$, we find

$$\mathfrak{r}_{(1)}=-\frac{C^{(\pm)}}{k^2}\sin^2\frac{k\tau}{2}+\frac{(-1)^n C^{(\pm)}}{k^2-4(\mathfrak{w}_{\rm dS}-\mathfrak{w}_{\rm R})^2}\times\sin\left[\left(\mathfrak{w}_{\rm dS}-\mathfrak{w}_{\rm R}+\frac{k}{2}\right)\tau\right]\sin\left[\left(\mathfrak{w}_{\rm dS}-\mathfrak{w}_{\rm R}-\frac{k}{2}\right)\tau\right], \tag{A10}$$

where $n=2m$ or $2m+1$. As a result, $\mathfrak{r}_{(1)}$ oscillates around zero. As for the other variables $\mathfrak{t}_{(1)},\theta_{(1)},\varphi_{(1)}$, although some of them may diverge as $\tau\to\infty$, no singularity appears in the evolution equations. Hence, we conclude that the coplanar circular orbit is linearly stable.

APPENDIX B: PLANETARY EQUATIONS FOR A BINARY SYSTEM IN NEWTONIAN LIMIT

In order to understand our numerical results, it may be better to introduce the Lagrange planetary equations, which give time evolution of the orbital parameters such as the semimajor axis, eccentricity, and inclination. To derive the planetary equations, we treat the proper Hamiltonian with unit mass $\mu=1$, which is given by

$$\bar{\mathcal{H}}=\bar{\mathcal{H}}_0+\bar{\mathcal{H}}_1,$$

where

$$\bar{\mathcal{H}}_0=\frac{1}{2}\bar{\mathsf{p}}^2-\frac{G(m_1+m_2)}{\mathsf{r}},$$
$$\bar{\mathcal{H}}_1=\bar{\mathcal{H}}_{\text{1-dS}}+\bar{\mathcal{H}}_{1-\bar{\mathcal{R}}},$$

with

$$\bar{\mathcal{H}}_{\text{1-dS}}=\mathfrak{w}_{\rm dS}(\bar{\mathsf{p}}_{\mathsf{y}}\mathsf{x}-\bar{\mathsf{p}}_{\mathsf{x}}\mathsf{y}),$$
$$\bar{\mathcal{H}}_{1-\bar{\mathcal{R}}}=\frac{\mathfrak{r}_g}{4\mathfrak{r}_0^3}\Big[\mathsf{x}^2+\mathsf{y}^2+\mathsf{z}^2-3(1+\mathfrak{r}_0^2\mathfrak{w}_0^2)(\mathsf{x}\cos\mathfrak{w}_{\rm R}\tau-\mathsf{y}\sin\mathfrak{w}_{\rm R}\tau)^2+3\mathfrak{r}_0^2\mathfrak{w}_0^2\mathsf{z}^2\Big].$$

The position $\mathsf{r}=(\mathsf{x},\mathsf{y},\mathsf{z})$ of a binary should be described in the nonrotating proper reference frame.

For the unperturbed Hamiltonian $\bar{\mathcal{H}}_0$, it is just the same as that of a binary in Newtonian dynamics. We find an elliptic orbit, which is described by

$$\mathsf{r}=\frac{a(1-e^2)}{1+e\cos f}, \tag{B1}$$

where r, a, e, and f are the radial distance from the center of mass, the semimajor axis, the eccentricity, and the true anomaly. This orbital plane is inclined with the inclination angle I from the equatorial plane in the proper reference frame.

Hence, the relative position $\mathsf{r}=(\mathsf{x},\mathsf{y},\mathsf{z})$ of a binary is given by the orbital parameters (ω,Ω,a,e,I,f) as Eq. (5.9) with Eq. (B1). Introducing the Delaunay variables as

$$\begin{cases}\mathfrak{l}=n(t-t_0)\\ \mathfrak{g}=\omega\\ \mathfrak{h}=\Omega\end{cases}\quad\text{and}\quad\begin{cases}\mathfrak{L}=\sqrt{G(m_1+m_2)a}\\ \mathfrak{G}=\sqrt{G(m_1+m_2)a(1-e^2)}\\ \mathfrak{H}=\sqrt{G(m_1+m_2)a(1-e^2)}\cos I\end{cases},$$

where

$$n\equiv\frac{2\pi}{P}=\sqrt{\frac{G(m_1+m_2)}{a^3}},$$

is the mean motion, we find the new unperturbed Hamiltonian to be

$$\tilde{\bar{\mathcal{H}}}_0=-\frac{G^2(m_1+m_2)^2}{2\mathfrak{L}^2}.$$

Including the perturbations $\bar{\mathcal{H}}_1$, we obtain the Hamiltonian by the Delaunay variables as

$$\tilde{\bar{\mathcal{H}}}=\tilde{\bar{\mathcal{H}}}_0+\bar{\mathcal{H}}_1.$$

After some calculations, the Hamilton equations are reduced to

$$\dot{a}=-\frac{2}{na}\frac{\partial\bar{\mathcal{H}}_1}{\partial\mathfrak{l}}, \tag{B2}$$

$$\dot{e}=\frac{\sqrt{1-e^2}}{na^2e}\frac{\partial\bar{\mathcal{H}}_1}{\partial\omega}-\frac{1-e^2}{na^2e}\frac{\partial\bar{\mathcal{H}}_1}{\partial\mathfrak{l}}, \tag{B3}$$

$$\dot{I}=\frac{1}{na^2\sin I\sqrt{1-e^2}}\frac{\partial\bar{\mathcal{H}}_1}{\partial\Omega}-\frac{\cos I}{na^2\sin I\sqrt{1-e^2}}\frac{\partial\bar{\mathcal{H}}_1}{\partial\omega}, \tag{B4}$$

$$\dot{\mathfrak{l}}=n+\frac{2}{na}\frac{\partial\bar{\mathcal{H}}_1}{\partial a}+\frac{1-e^2}{na^2e}\frac{\partial\bar{\mathcal{H}}_1}{\partial e}, \tag{B5}$$

$$\dot{\omega}=-\frac{\sqrt{1-e^2}}{na^2e}\frac{\partial\bar{\mathcal{H}}_1}{\partial e}+\frac{\cos I}{na^2\sin I\sqrt{1-e^2}}\frac{\partial\bar{\mathcal{H}}_1}{\partial I}, \tag{B6}$$

$$\dot{\Omega}=-\frac{1}{na^2\sin I\sqrt{1-e^2}}\frac{\partial\bar{\mathcal{H}}_1}{\partial I}. \tag{B7}$$

The partial derivative $\partial/\partial\mathfrak{l}$ can be replaced by that of the true anomaly as

$$\frac{\partial}{\partial \mathfrak{l}} = (1-e^2)^{-\frac{3}{2}}(1+e\cos f)^2\frac{\partial}{\partial f}.$$

Hence, once we find the perturbation Hamiltoninan $\bar{\mathcal{H}}_1$ in terms of the orbital parameters, we obtain the planetary equations.

The proper Hamiltonian is described by the orbital parameters by inserting the relation given in Eq. (5.9) with Eq. (B1). We then find the perturbed Hamiltonian as

$$\bar{\mathcal{H}}_1 = \bar{\mathcal{H}}_{1\text{-dS}} + \bar{\mathcal{H}}_{1\text{-}\bar{\mathcal{R}}},$$

where

$$\bar{\mathcal{H}}_{1-\text{dS}} = \mathfrak{w}_{\text{dS}}\mathfrak{r}^2(a,e,f)\Big\{n\cos I(1-e^2)^{-3/2}(1+e\cos f)^2 - \mathfrak{w}_{\text{dS}}\Big(\cos^2(\omega+f)+\sin^2(\omega+f)\cos^2 I\Big)\Big\} \tag{B8}$$

$$\bar{\mathcal{H}}_{1-\bar{\mathcal{R}}} = \frac{\mathfrak{r}_g}{4\mathfrak{r}_0^3}\mathfrak{r}^2(a,e,f)\Big\{1-3(1+\mathfrak{r}_0^2\mathfrak{w}_0^2)[\cos(\Omega+\mathfrak{w}_{\text{R}}\tau) \times\cos(\omega+f)-\sin(\Omega+\mathfrak{w}_{\text{R}}\tau)\sin(\omega+f)\cos I]^2 + 3\mathfrak{r}_0^2\mathfrak{w}_0^2\sin^2(\omega+f)\sin^2 I\Big\}. \tag{B9}$$

We then obtain the planetary equations for the present hierarchical triple system from Eqs. (B2)–(B7).

1. Double-averaging approach

Here, instead of solving the Lagrange planetary equations themselves, which is equivalent to our numerical methods in the text, we take the average of the perturbed Hamiltonian over two periods, the inner and outer orbital periods, and then analyze the simplified equations, because we are interested in the long-time behavior of the present system such as the vZLK mechanism.

The double-averaged Hamiltonian is defined by

$$\langle\langle\bar{\mathcal{H}}_1\rangle\rangle \equiv \frac{1}{2\pi}\int_0^{2\pi} d\mathfrak{l}_{\text{out}}\left(\frac{1}{2\pi}\int_0^{2\pi} d\mathfrak{l}\bar{\mathcal{H}}_1\right).$$

Since the outer orbit is circular, we find that $\mathfrak{l}_{\text{out}} = f_{\text{out}} = \mathfrak{w}_0\tau$. We also have

$$d\mathfrak{l} = \frac{1}{\sqrt{1-e^2}}\left(\frac{\mathfrak{r}}{a}\right)^2 df.$$

Inserting Eqs. (B8) and (B9) into the above integrals, we find the doubly-averaged Hamiltonian as

$$\langle\langle\bar{\mathcal{H}}_1\rangle\rangle = \mathfrak{w}_{\text{dS}}na^2\sqrt{1-e^2}\cos I - \frac{a^2}{8}\left\{(2+3e^2)\left[\mathfrak{w}_{\text{dS}}^2(3+\cos 2I)+\frac{\mathfrak{r}_g}{8\mathfrak{r}_0^3}(1+3\mathfrak{r}_0^2\mathfrak{w}_0^2)(1+3\cos 2I)\right] + 10e^2\sin^2 I\cos 2\omega\left[\mathfrak{w}_{\text{dS}}^2+\frac{3\mathfrak{r}_g}{8\mathfrak{r}_0^3}(1+3\mathfrak{r}_0^2\mathfrak{w}_0^2)\right]\right\}. \tag{B10}$$

Using the doubly-averaged Hamiltonian Eq. (B10), we obtain the Lagrange planetary equations as

$$\dot{e} = \frac{5}{4}\left(\mathfrak{w}_{\text{dS}}^2+\frac{3\mathfrak{r}_g}{8\mathfrak{r}_0^3}(1+3\mathfrak{r}_0^2\mathfrak{w}_0^2)\right)\frac{e\sqrt{1-e^2}}{n}(1-\cos 2I)\sin(2\omega), \tag{B11}$$

$$\dot{I} = -\frac{5}{4}\left(\mathfrak{w}_{\text{dS}}^2+\frac{3\mathfrak{r}_g}{8\mathfrak{r}_0^3}(1+3\mathfrak{r}_0^2\mathfrak{w}_0^2)\right)\frac{e^2}{n\sqrt{1-e^2}}\sin 2I\sin(2\omega), \tag{B12}$$

$$\dot{\omega} = \frac{1}{4n}\left(\mathfrak{w}_{\text{dS}}^2+\frac{3\mathfrak{r}_g}{8\mathfrak{r}_0^3}(1+3\mathfrak{r}_0^2\mathfrak{w}_0^2)\right)\left[\sqrt{1-e^2}[3+5\cos 2I+5(1-\cos 2I)\cos 2\omega]+\frac{5e^2}{\sqrt{1-e^2}}(1+\cos 2I)(1-\cos 2\omega)\right] + \frac{2\sqrt{1-e^2}}{n}\mathfrak{w}_{\text{dS}}^2, \tag{B13}$$

$$\dot{\Omega} = \mathfrak{w}_{\text{dS}} + \frac{\cos I}{2n\sqrt{1-e^2}}\left(\mathfrak{w}_{\text{dS}}^2+\frac{3}{8}\frac{\mathfrak{r}_g}{\mathfrak{r}_0^3}(1+3\mathfrak{r}_0^2\mathfrak{w}_0^2)\right)[-(2+3e^2)+5e^2\cos(2\omega)]. \tag{B14}$$

The semimajor axis a is constant in the present approximation. Also, we can easily check from Eqs. (B11) and (B12) that

$$\frac{d}{d\tau}(\sqrt{1-e^2}\cos I) = 0,$$

which corresponds to conservation of the z-component of the angular momentum.

2. vZLK oscillations

Introducing a "potential" by $V_S \equiv -\langle\langle \bar{\mathcal{H}}_1 \rangle\rangle$, we rewrite the above planetary equations as

$$\dot{e} = -\frac{\sqrt{1-e^2}}{na^2 e}\frac{\partial V_S}{\partial \omega}, \tag{B15}$$

$$\dot{I} = \frac{\cos I}{na^2 \sin I\sqrt{1-e^2}}\frac{\partial V_S}{\partial \omega}, \tag{B16}$$

$$\dot{\omega} = \frac{\sqrt{1-e^2}}{na^2 e}\frac{\partial V_S}{\partial e} - \frac{\cos I}{na^2 \sin I\sqrt{1-e^2}}\frac{\partial V_S}{\partial I}, \tag{B17}$$

$$\dot{\Omega} = \frac{1}{na^2 \sin I\sqrt{1-e^2}}\frac{\partial V_S}{\partial I}. \tag{B18}$$

We obtain the closed form of a set of the differential equations for e, I, and ω by Eqs. (B15), (B16), and (B17). It gives several properties of vZLK oscillations such as the oscillation amplitude of the eccentricity and the oscillation timescale as analyzed in the Newtonian and 1PN hierarchical triple system [46].

The potential is written by use of $\eta \equiv \sqrt{1-e^2}$ and $\mu_I \equiv \cos I$ as

$$V_S \equiv -\langle\langle \bar{\mathcal{H}}_1 \rangle\rangle = \frac{a^2 \mathfrak{r}_g(1+3\mathfrak{r}_0^2\mathfrak{w}_0^2)}{32\mathfrak{r}_0^3} v_S(\eta, \mu_I),$$

where

$$v_S(\eta,\mu_I) \equiv 2(-1+3\mu_I^2\eta^2)(1+\alpha_{\rm dS}) + 12C_{\rm KL} + 4\alpha_{\rm dS}\left(2 - \frac{3n}{\mathfrak{w}_{\rm dS}}\mu_I\eta\right),$$

with

$$\alpha_{\rm dS} \equiv \frac{8\mathfrak{w}_{\rm dS}^2\mathfrak{r}_0^3}{3\mathfrak{r}_g(1+3\mathfrak{r}_0^2\mathfrak{w}_0^2)},$$

$$C_{\rm KL} \equiv (1-\eta^2)\left[(1+2\alpha_{\rm dS}) - \frac{5}{2}(1+\alpha_{\rm dS})(1-\mu_I^2)\sin^2\omega\right].$$

Note that when $\alpha_{\rm dS} = 0$, we find the same equations for the Newtonian hierarchical triple system with quadrupole approximation. The terms with $\alpha_{\rm dS}$ give relativistic corrections.

Introducing the normalized time $\tilde{\tau}$, which is defined by

$$\tilde{\tau} \equiv \frac{\tau}{\tau_{\rm vZLK}},$$

with the typical vZLK timescale

$$\tau_{\rm vZLK} \equiv \frac{32n\mathfrak{r}_0^3}{\mathfrak{r}_g(1+3\mathfrak{r}_0^2\mathfrak{w}_0^2)}\left(\sim\frac{P_{\rm out}^2}{P_{\rm in}}\right),$$

the above planetary equation is rewritten as

$$\frac{d\eta}{d\tilde{\tau}} = \frac{\partial v_S}{\partial \omega},$$
$$\frac{1}{\mu_I}\frac{d\mu_I}{d\tilde{\tau}} = -\frac{1}{\eta}\frac{\partial v_S}{\partial \omega},$$
$$\frac{d\omega}{d\tilde{\tau}} = -\frac{\partial v_S}{\partial \eta} + \frac{\mu_I}{\eta}\frac{\partial v_S}{\partial \mu_I}.$$

From these equations, we can easily show that

$$\frac{d(\mu_I\eta)}{d\tilde{\tau}} = 0, \qquad \frac{dv_S}{d\tilde{\tau}} = 0,$$

which means there exist two conserved quantities $\vartheta \equiv \mu_I\eta$ and $C_{\rm KL}$ just as the Newtonian and 1PN hierarchical triple system under dipole approximation. Using these two conserved quantities, we obtain a single equation for η as

$$\frac{d\eta^2}{d\tilde{\tau}} = -24\sqrt{2}\sqrt{f(\eta^2)g(\eta^2)},$$

with

$$f(\eta^2) \equiv (1+2\alpha_{\rm dS})(1-\eta^2) - C_{\rm KL},$$
$$g(\eta^2) \equiv -5(1+\alpha_{\rm dS})\vartheta^2 + [5(1+\alpha_{\rm dS})\vartheta^2 + 3 + \alpha_{\rm dS} + 2C_{\rm KL}]\eta^2 - (3+\alpha_{\rm dS})\eta^4.$$

Setting $\xi = \eta^2$, we find

$$\frac{d\xi}{d\tilde{\tau}} = -24\sqrt{2(1+2\alpha_{\rm dS})(3+\alpha_{\rm dS})}\sqrt{(\xi-\xi_0)(\xi-\xi_+)(\xi-\xi_-)},$$

where

$$\xi_0 = 1 - \frac{C_{\rm KL}}{1+2\alpha_{\rm dS}},$$

$$\xi_\pm = \frac{1}{2}\left[\left(1+\frac{5(1+\alpha_{\rm dS})}{3+\alpha_{\rm dS}}\vartheta^2+\frac{2}{3+\alpha_{\rm dS}}C_{\rm KL}\right) \pm \sqrt{\left(1+\frac{5(1+\alpha_{\rm dS})}{3+\alpha_{\rm dS}}\vartheta^2+\frac{2}{3+\alpha_{\rm dS}}C_{\rm KL}\right)^2 - \frac{20(1+\alpha_{\rm dS})}{3+\alpha_{\rm dS}}\vartheta^2}\right],$$

are the solutions of $f(\xi)=0$ and $g(\xi)=0$, respectively.

We can find the relativistic corrections with $\alpha_{\rm dS}$, which is evaluated as

$$\alpha_{\rm dS} = \frac{3\mathfrak{r}_g^2}{\mathfrak{r}_0^2\left(1+\sqrt{1-\frac{3\mathfrak{r}_g}{2\mathfrak{r}_0}}\right)^2} \le \frac{1}{3\left(1+\frac{1}{\sqrt{2}}\right)^2} \approx 0.114382.$$

The equality is found in the case of the ISCO radius ($\mathfrak{r}_0 = 3\mathfrak{r}_g$).

Analyzing the above equation, we find that there exists vZLK oscillation in this system just the same as in Newtonian hierarchical triple system, and we can classify the vZLK solutions by the sign of $C_{\rm KL}$ into two cases: (1) $C_{\rm KL} > 0$ (rotation) and (2) $C_{\rm KL} < 0$ (libration).

a. $C_{\rm KL} > 0$ (rotation)

In this case, $0 < \xi_- < 1 < \xi_+$ and $0 < \xi_0 < 1$. This is possible if

$$0 < C_{\rm KL} < 1 + 2\alpha_{\rm dS}.$$

Hence we find the maximum and minimum values of the eccentricity as

$$e_{\rm max} = \sqrt{1-\xi_-}, \qquad e_{\rm min} = \sqrt{1-\xi_0}.$$

The vZLK timescale is given by

$$T_{\rm vZLK} = \tau_{\rm vZLK}\mathfrak{T}^{(rot)}_{\rm vZLK}, \tag{B19}$$

where

$$\mathfrak{T}^{(rot)}_{\rm vZLK} \equiv \frac{1}{12\sqrt{2(1+2\alpha_{\rm dS})(3+\alpha_{\rm dS})}} \times \int_{\xi_-}^{\xi_0} d\xi \frac{1}{\sqrt{(\xi-\xi_0)(\xi-\xi_+)(\xi-\xi_-)}}. \tag{B20}$$

b. $C_{\rm KL} < 0$ (libration)

Since $0 < \xi_- < \xi_+ < 1$ and $\xi_0 < 0$ in this case, we find

$$e_{\rm max} = \sqrt{1-\xi_-}, \qquad e_{\rm min} = \sqrt{1-\xi_+}.$$

It occurs when

$$-\frac{3+\alpha_{\rm dS}}{2} < C_{\rm KL} < 0, \quad \text{and} \quad \vartheta < \frac{(\sqrt{3+\alpha_{\rm dS}} - \sqrt{-2C_{\rm KL}})}{\sqrt{5(1+\alpha_{\rm dS})}}.$$

The vZLK timescale is given by

$$T_{\rm vZLK} = \tau_{\rm vZLK}\mathfrak{T}^{(lib)}_{\rm vZLK}, \tag{B21}$$

where

$$\mathfrak{T}^{(lib)}_{\rm vZLK} \equiv \frac{1}{12\sqrt{2(1+2\alpha_{\rm dS})(3+\alpha_{\rm dS})}} \times \int_{\xi_-}^{\xi_+} d\xi \frac{1}{\sqrt{(\xi-\xi_0)(\xi-\xi_+)(\xi-\xi_-)}}. \tag{B22}$$

The maximum and minimum values of the eccentricity in the vZLK oscillations are determined by two conserved parameters, ϑ and $C_{\rm KL}$. We present one example in Fig. 11. We choose $\vartheta = 0.5$ and show the maximum value, $e_{\rm max}$ (the red curve), and the minimum value, $e_{\rm min}$ (the blue curve), in terms of $C_{\rm KL}$. The solid curves denote the case of $\alpha_{\rm dS} = 0.0794$ (model I), while the dotted curves is the case of $\alpha_{\rm dS} = 0$. For model Ic, we find $C_{\rm KL} = -0.0000359$, which is consistent with our result in Table I. The relativistic effect with $\alpha_{\rm dS}$ is small.

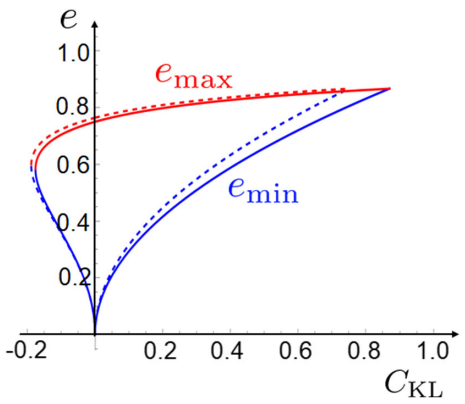

FIG. 11. The maximum and minimum values of the eccentricity in vZLK oscillations. We choose $\vartheta = 0.5$. The red and blue curves depict the maximum and minimum values, respectively. The solid curves denote the case of $\alpha_{\rm dS} = 0.0794$ (model I). We also show the case of $\alpha_{\rm dS} = 0$ by the dotted curves.

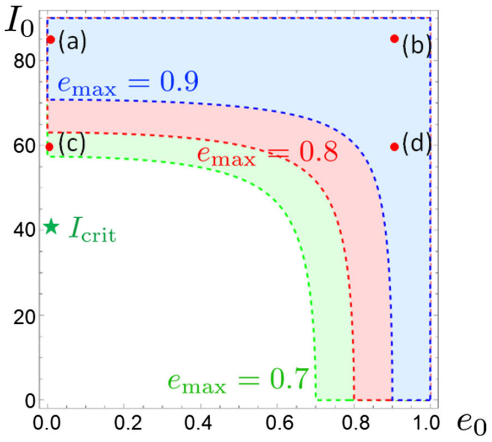

FIG. 12. The range of the initial conditions (e_0 and I_0) for the large maximum values of the eccentricity. The light blue, light red, and light green regions correspond to the regions of $0.9 \le e_{\max} < 1.0$, $0.8 \le e_{\max} < 0.9$, and $0.7 \le e_{\max} < 0.8$, respectively. The red dots denote models a, b, c, and d. The critical angle is also shown by the green star.

The maximum eccentricity in vZLK oscillations is important, especially when we discuss emission of GWs. We plot the range of the initial conditions (e_0 and I_0) which show the large maximum values of the eccentricity in Fig. 12. The light blue, light red, and light green regions correspond to $0.9 \le e_{\max} < 1.0$, $0.8 \le e_{\max} < 0.9$, and $0.7 \le e_{\max} < 0.8$, respectively. The red dots denote models a, b, c, and d. Note that this figure is valid for models I, II, and III. Hence, when the initial inclination angle is large, the maximum eccentricity may grow close to unity.

The timescale of the vZLK oscillations is important for observation of the gravitational waves. From Eqs. (B20) and (B22), assuming the integrals do not so much depend on the relativistic parameters, we may roughly evaluate the relativistic effect (including de Sitter precession), which is given by

$$\frac{T_{\rm vZLK}}{T^{(N)}_{\rm vZLK}} \approx \frac{1 + 3\mathfrak{r}_0^2\mathfrak{w}_0^2}{\sqrt{(1+2\alpha_{\rm dS})(1+\alpha_{\rm dS}/3)}},$$

where $T^{(N)}_{\rm vZLK}$ is the Newtonian value. This ratio changes from 0.4427 to 1 as $\mathfrak{r}_0$ increases from the ISCO radius to infinity. Hence, the vZLK timescale near the ISCO radius may become smaller than one half of the Newtonian value.

We can also evaluate a critical inclination angle, beyond which the vZLK oscillation occurs even when the initial eccentricity is very small. It is given by the condition for a bifurcation point with $C_{\rm KL} = 0$ with $\omega = 90°$. Setting

$$(1+2\alpha_{\rm dS}) - \frac{5}{2}(1+\alpha_{\rm dS})\sin^2 I_{\rm crit} = 0,$$

we obtain

$$I_{\rm crit} = \sin^{-1}\sqrt{\frac{2(1+2\alpha_{\rm dS})}{5(1+\alpha_{\rm dS})}}.$$

We find that the critical inclination angle changes from 41.6° to the Newtonian value $I^{(N)}_{\rm crit} = \sin^{-1}\sqrt{2/5} \approx 39.2°$ as $\mathfrak{r}_0$ increases from the ISCO radius to infinity.

[1] B. P. Abbott, R. Abbott, T. D. Abbott, S. Abraham, F. Acernese, K. Ackley, C. Adams, V. B. Adya, C. Affeldt *et al.*, Living Rev. Relativity **23**, 1 (2020).
[2] B. P. Abbott, R. Abbott, T. D. Abbott, S. Abraham, F. Acernese, K. Ackley, C. Adams, V. B. Adya, C. Affeldt *et al.*, SoftwareX **13**, 100658 (2021).
[3] The LIGO Scientific, the Virgo, and the KAGRA Collaborations, Phys. Rev. X **9**, 031040 (2019).
[4] The LIGO Scientific, the Virgo, and the KAGRA Collaborations, arXiv:2302.03676.
[5] LIGO Scientific and Virgo Collaboration, Phys. Rev. Lett. **116**, 061102 (2016).
[6] LIGO Scientific and Virgo Collaboration, Phys. Rev. Lett. **119**, 161101 (2017).
[7] The LIGO Scientific and the Virgo Collaborations, Phys. Rev. D **100**, 104036 (2019).
[8] The LIGO Scientific and the Virgo Collaborations, Astrophys. J. **900**, L13 (2020).
[9] The LIGO Scientific and the Virgo Collaborations, Phys. Rev. D **103**, 122002 (2021).
[10] The LIGO Scientific and the Virgo Collaborations, Astrophys. J. Lett. **913**, L7 (2021).
[11] The LIGO Scientific, the Virgo, and the KAGRA Collaborations, arXiv:2111.03604.
[12] D. C. Heggie, Mon. Not. R. Astron. Soc. **173**, 729 (1975).
[13] P. Hut, Astrophys. J. **403**, 256 (1993).
[14] J. Samsing, M. MacLeod, and E. Ramirez-Ruiz, Astrophys. J. **784**, 71 (2014).
[15] R. L. Riddle *et al.*, Astrophys. J. **799**, 4 (2015).
[16] F. Antonini, S. Chattejee, C. Rodriguez, M. Morscher, B. Pattabiraman, V. Kalogera, and F. Rasio, Astrophys. J. **816**, 2 (2016).
[17] A. P. Stephan, S. Naoz, A. M. Ghez, M. R. Morris, A. Ciurlo, T. Do, K. Breivik, S. Coughlin, and C. L. Rodriguez, Astrophys. J. **878**, 58 (2019).
[18] M. Mapelli, F. Santoliquido, Y. Bouffanais, M. Arca Sedda, M. C. Artale, and A. Ballone, Symmetry **13**, 1678 (2021).
[19] V. Gayathri, I. Bartos, Z. Haiman, S. Klimenko, B. Kocsis, S. Márka, and Y. Yang, Astrophys. J. **890**, L20 (2020).
[20] D. Gerosa and M. Fishbach, Nat. Astron. **5**, 749 (2021).

[21] H. von Zeipel, Astron. Nachr. **183**, 345 (1910).
[22] Y. Kozai, Astron. J. **67**, 591 (1962).
[23] M. Lidov, Planet. Space Sci. **9**, 719 (1962).
[24] I. Shevchenko, *The Lidov-Kozai Effect-Applications in Exoplanet Research and Dynamical Astronomy* (Springer, New York, 2017).
[25] L. Randall and Z.-Z. Xianyu, arXiv:1902.08604.
[26] B. Hoang and S. Naoz, Astrophys. J. **852**, 2 (2018).
[27] P. Gupta, H. Suzuki, H. Okawa, and K. Maeda, Phys. Rev. D **101**, 104053 (2020).
[28] S. Naoz, B. Kocsis, A. Loeb, and N. Yunes, Astrophys. J. **773**, 187 (2013).
[29] S. Naoz, W. Farr, and F. Rasio, Astrophys. J. **754**, L36 (2012).
[30] S. Naoz, Annu. Rev. Astron. Astrophys. **54**, 441 (2016).
[31] S. Naoz, C. M. Will, E. Ramirez-Ruiz, A. Hees, A. M. Ghez, and T. Do, Astrophys. J. **888**, L8 (2019).
[32] J. Teyssandier, S. Naoz, I. Lizarraga, and F. A. Rasio, Astrophys. J. **779**, 169 (2013).
[33] G. Li, S. Naoz, B. Kocsis, and A. Loeb, Mon. Not. R. Astron. Soc. **451**, 1341 (2015).
[34] C. Will, Phys. Rev. D **89**, 044043 (2014).
[35] C. Will, Classical Quantum Gravity **31**, 244001 (2014).
[36] P. Amaro-Seoane, A. Sesana, L. Hoffman, M. Benacquista, C. Eichhorn, J. Makino, and R. Spurzem, Mon. Not. R. Astron. Soc. **402**, 2308 (2010).
[37] F. Antonini and H. Perets, Astrophys. J. **757**, 27 (2012).
[38] F. Antonini, S. Chatterjee, C. Rodriguez, M. Morscher, and B. Pattabiraman, Astrophys. J. **816**, 2 (2016).
[39] Y. Meiron, B. Kocsis, and A. Loeb, Astrophys. J. **84**, 2 (2017).
[40] T. Robson, N. Cornish, N. Tamanini, and S. Toonen, Phys. Rev. D **98**, 064012 (2018).
[41] L. Randall and Z.-Z. Xianyu, Astrophys. J. **878**, 75 (2019).
[42] B.-M. Hoang, S. Naoz, B. Kocsis, W. M. Farr, and J. McIver, Astrophys. J. Lett. **875**, L31 (2019).
[43] R. Emami and A. Loeb, Mon. Not. R. Astron. Soc. **495**, 536 (2020).
[44] A. Kuntz and K. Leyde, arXiv:2212.09753.
[45] H. Suzuki, P. Gupta, H. Okawa, and K. Maeda, Mon. Not. R. Astron. Soc. **486**, L1 (2019).
[46] H. Suzuki, P. Gupta, H. Okawa, and K. Maeda, Mon. Not. R. Astron. Soc. **500**, 1645 (2020).
[47] B. Liu, D. Lai, and Y.-H. Wang, Astrophys. J. Lett. **883**, L7 (2019).
[48] B. Liu and D. Lai, Astrophys. J. **924**, 127 (2022).
[49] H. Lim and C. L. Rodriguez, Phys. Rev. D **102**, 064033 (2020).
[50] F. K. Manasse and C. W. Misner, J. Math. Phys. (N.Y.) **4**, 735 (1963).
[51] A. I. Nesterov, Classical Quantum Gravity **16**, 465 (1999).
[52] P. Delva and M. C. Angonin, Gen. Relativ. Gravit. **44**, 1 (2012).
[53] P. Banerjee, S. Paul, R. Shaikh, and T. Sarkar, Phys. Lett. B **795**, 29 (2019).
[54] M. Ishii, M. Shibata, and Y. Mino, Phys. Rev. D **71**, 044017 (2005).
[55] R. M. Cheng and C. R. Evans, Phys. Rev. D **87**, 104010 (2013).
[56] A. Kuntz, F. Serra, and E. Trincherini, Phys. Rev. D **104**, 024016 (2021).
[57] A. Gorbatsievich and A. Bobrik, AIP Conf. Proc. **1205**, 87 (2010).
[58] X. Chen and Z. Zhang, Phys. Rev. D **106**, 103040 (2022).
[59] F. Camilloni, G. Grignani, T. Harmark, R. Oliveri, M. Orselli, and D. Pica, Phys. Rev. D **107**, 084011 (2023).
[60] C. W. Misner, K. S. Thorne, and J. A. Wheeler, *Gravitation* (Princeton university Press, USA, 1973).
[61] W. de Sitter, Mon. Not. R. Astron. Soc. **76**, 699 (1916).
[62] R. A. Mardling and S. J. Aarseth, Mon. Not. R. Astron. Soc. **321**, 398 (2001).
[63] A. Mylläri, M. Valtonen, A. Pasechnik, and S. Mikkola, Mon. Not. R. Astron. Soc. **476**, 830 (2018).
[64] C. M. Will, Classical Quantum Gravity **36**, 195013 (2019).
[65] J. Antognini, Mon. Not. R. Astron. Soc. **452**, 3610 (2015).
[66] M. Maggiore, *Gravitational Waves: Volume 1: Theory and Experiments* (Oxford University Press, New York, 2007), ISBN 9780198570745.
[67] P. C. Peters and J. Mathews, Phys. Rev. **131**, 435 (1963).
[68] V. Cardoso, F. Duque, and G. Khanna, Phys. Rev. D **103**, L081501 (2021).
[69] Y. Lithwick and S. Naoz, Astrophys. J. **742**, 94 (2011).
[70] B. Katz, S. Dong, and R. Malhotra, Phys. Rev. Lett. **107**, 181101 (2011).
[71] S. Naoz, W. M. Farr, Y. Lithwick, F. A. Rasio, and J. Teyssandier, Mon. Not. R. Astron. Soc. **431**, 2155 (2013).
[72] G. Li, S. Naoz, B. Kocsis, and A. Loeb, Astrophys. J. **785**, 116 (2014).
[73] B. Liu, D. J. Muñoz, and D. Lai, Mon. Not. R. Astron. Soc. **447**, 747 (2015).